Chapter 3

PHYSICO – CHEMICAL CHARACTERIZATION

Contents

Transition metals incorporated mesoporous ceria catalysts were prepared by the soft templated method using the neutral surfactant hexadecyl amine (HDA). A detailed investigation of physico-chemical characterization of the catalytic systems was performed by techniques such as wide and low angle XRD, BET surface area, pore volume and pore distribution by sorption studies of nitrogen gas, EDX, ICP-AES, SEM, TEM, TG/DTA, UV-Vis DRS, FT-IR and temperature programmed reduction-hydrogen (TPR-H_2). Surface acidic properties of the systems were obtained from TPD of ammonia, and the results were tested by the test reaction of vapour phase cumene cracking.

3.1 Introduction

Porous materials have attracted the attention of chemists and material scientists due to commercial interest in their application in chemical separations and heterogeneous catalysis as well as scientific interest in the challenges posed by their synthesis, processing and characterization in heterogeneous catalysis. Catalysis and catalytic surfaces are needed to be characterized with reference to their physical properties and thereby investigating their actual performance as catalysts. The most important physical properties are those relating to the surface because catalytic performance is determined by the surface parameters. A complete knowledge on the exact location, structure and electronic ground state of the active site in the catalysts is essential to establish a basic understanding about the structure- activity correlations and to improve the efficiency of the catalyst for higher selectivity and stability [1]. Again variation in the conditions of preparation and pre-treatment very much alters the surface properties and the catalytic behaviour of the catalysts.

In recent years a considerable amount of interest has been shown in materials with grain size in nano scale. Preparation of nano size mesoporous cerium oxide was done by surfactant method and transition metals incorporated mesoporous cerium oxide catalysts were prepared by wet impregnation method. After catalyst preparation, the removal of surfactant from calcined sample was confirmed by FT-IR. FT-IR also give knowledge about surface functional groups. The surface morphology was obtained from SEM and TEM. Surface areas of the systems were measured by BET surface area measurement. Pore volume, pore size distribution and mesoscopic nature were investigated by sorption studies of nitrogen gas at liquid nitrogen temperature. Phase formation and

mesoscopic nature of ceria crystals and modified samples were tested by wide and low angle XRD. Thermal stability of the systems were analysed by thermo gravimetric analysis. XRD study was performed to understand chemical structure of the prepared systems. UV-Vis-Diffuse reflectance spectrum gives idea about the metal ion co-ordination. Temperature programmed desorption of ammonia was carried out to understand the amount, distribution and strength of the acid sites of the prepared systems. Acidity thus obtained was tested by vapour phase cumene cracking reaction.

3.2 Physico - Chemical Characterization

The catalyst samples prepared were characterized by adopting various physical methods such as BET Surface area, pore diameter, pore distribution and pore volume measurements by BJH sorption studies of nitrogen, low and wide angle XRD, FT-IR, SEM, EDX, TEM, TG/DTA, ICP–AES, TPR in H_2 and UV-Vis DRS. The observations and explanations are given below.

3.2.1 Energy Dispersive X-ray Analysis (EDAX)

The knowledge of solid chemical composition must be the starting point of every investigation. A lot of literature results cannot be evaluated because of lack of composition data. It is noteworthy to remember that: (i) catalyst composition at the end of preparation can be different from that calculated from the weight of reagents; this is frequently observed in co-precipitation, hydrothermal synthesis, calcination of solids containing volatile compounds; (ii) composition reproducibility is a very common problem in catalyst preparation, so frequent experimental checks are necessary; (iii) impurities can always be present; their origin is extremely

variable as they can come from polluted reagents, previous preparation residues, release of substances from vessels, etc. (iv) exposure to the reaction atmosphere changes almost every time the catalyst composition because of loss of volatile compounds, deposition of organic substances, reactions between solid and environment.

Energy dispersive X-ray spectroscopy (EDX) measurements and qualitative elemental analysis made on the calcined samples show the expected primary metal element signals which confirm that the inorganic walls consist of predominantly metal-oxygen networks. The elemental composition of the manganese doped and chromium doped samples were determined using EDX analysis and the results for a few samples are given in Fig.3.1.

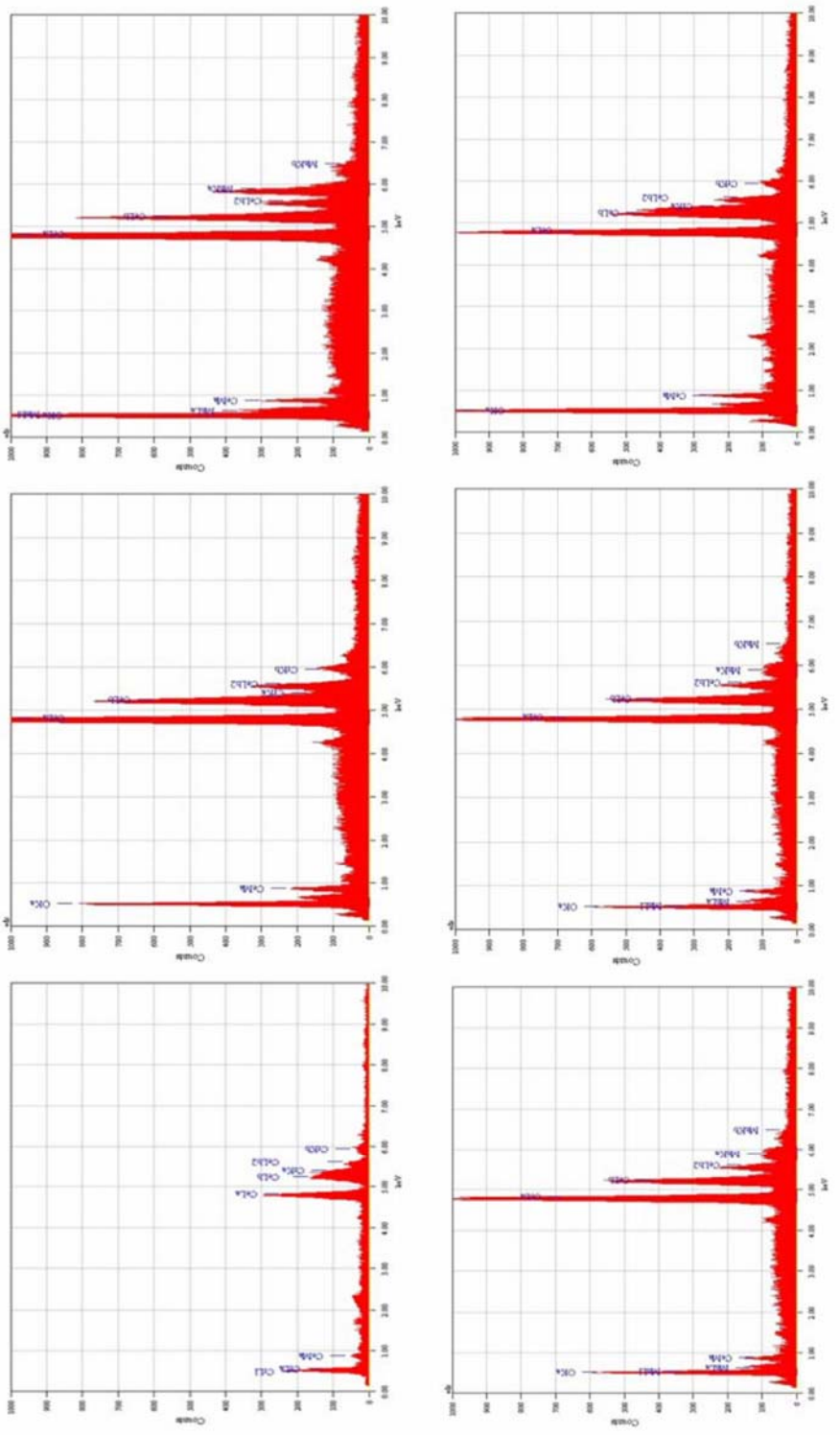

Fig. 3.1 EDX data for Manganese and Chromium modified catalyst systems

3.2.2 Elemental Analysis – ICP-AES Analysis

Table 3.1 Composition (Atom %) of prepared samples

Catalysts	Composition (Atom %)			
	Ce		Metal	
	Theoretical	experimental	Theoretical	experimental
CeCr (2%)	93.7	94.7	6.3	5.3
CeCr (4%)	87.8	86.6	12.2	13.4
CeCr (10%)	73.1	76.3	26.9	23.7
CeFe (2%)	94.1	93.6	5.9	6.4
CeFe (4%)	88.6	87.9	11.4	12.1
CeFe (10%)	74.5	74	25.5	26
CeMn (2%)	94	93.2	6	6.8
CeMn (4%)	88.4	87.1	11.6	12.9
CeMn (10%)	74.4	73.4	25.6	26.6
CeCo (2%)	94.4	94	5.6	6
CeCo (4%)	89.1	89.2	10.9	10.8
CeCo (10%)	75.5	75.3	24.5	24.7
CeCu (2%)	94.7	94.6	5.3	5.4
CeCu (4%)	89.9	89.2	10.1	10.8
CeCu (10%)	76.9	76	23.9	24
CeNi(2%)	94.3	94.5	5.7	5.5
CeNi (4%)	89.1	89.1	10.9	10.9
CeNi (10%)	75.5	75.5	24.5	24.5

Various transition metal modified mesoporous ceria with various percentages of metals were synthesized and elemental analysis was done using ICP-AES. The data shown in the Table 3.1 gives the amount of CeO_2 and the different metals present in each samples. It is observed that the experimental atom percentage is close to the theoretical values. It can be concluded that the method of preparation adopted is effective for the preparation of metal modified ceria catalysts with required composition.

3.2.3 Surface area and pore volume measurements

The BET surface area (S_{BET}) and pore volumes measured for mesoporous ceria calcined at different temperatures are given in the Table 3.2.

Table 3.2 Surface area and pore volumes of mesoporous ceria

catalyst	S_{BET}(m^2 g^{-1})	Pore volume (cm^3 g-1)	Pore diameter(nm)
Ce-250	61	0.26	4.8
Ce-350	164	0.29	4.6
Ce-400	134	0.17	4.8
Ce-500	108	0.15	5.2
Ce-550	105	0.19	4.7
Ce-600	79	0.18	5.2

* Pore volume measured at p/p_0 of 0.997

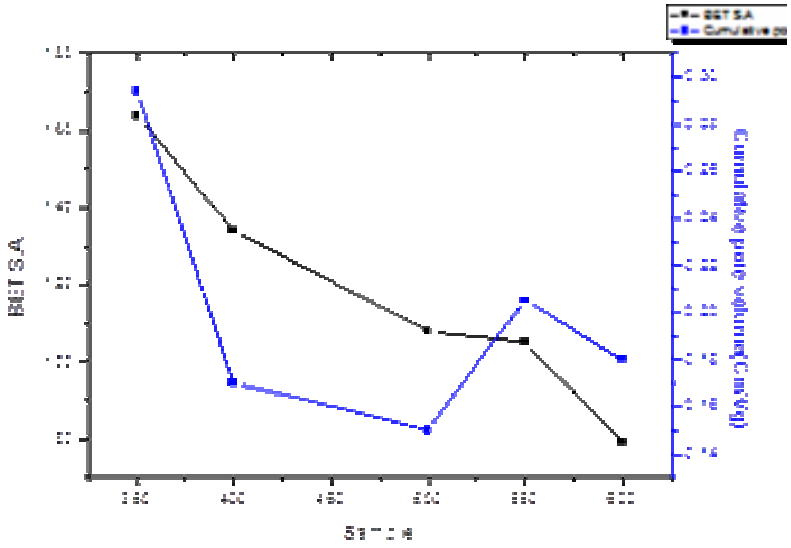

Fig.3.2 Variation of surface area and pore volume with calcination temperature

From the Table 3.2 it can be observed that as the calcination temperature increases the surface area decreases. There is change in the pore

volume with calcination temperature. The material showed a high (BET) surface area of 164 m^2g^{-1}. In the literature, most of the publications report ceria with specific surface areas below 100 m^2g^{-1} and only in a few cases was values around 200 m^2g^{-1} were obtained [2].

Table 3.3 Surface area and pore volume of metal incorporated mesoporous ceria systems

Catalyst	S_{BET}(m^2 g^{-1})	Pore volume (cm^3 g^{-1})	Pore diameter(nm)
Ce-350	164	0.29	4.6
CeCr (2%)	123	0.2	5.4
CeCr (4%)	120	0.18	5.6
CeCr (10%)	96	0.14	3.8
CeFe (2%)	100	0.18	4.5
CeFe (4%)	99	0.17	5.2
CeFe (10%)	52.6	0.12	4.6
CeCo (2%)	135	0.22	4.59
CeCo (4%)	124	0.19	4.99
CeCo (10%)	108	0.17	4.69
CeMn (2%)	121	0.23	4.71
CeMn(4%)	119	0.22	4.92
CeMn(10%)	109	0.18	4.5
CeCu (2%)	82	0.18	4.4
CeCu (4%)	80	0.17	5.2
CeCu (10%)	72	0.15	4.3
CeNi (2%)	96	0.18	4.6
CeNi (4%)	89	0.15	4.4
CeNi (10%)	85	0.14	3.8

* Pore volume measured at p/p_0 of 0.997

The surface areas decrease with metal loading and increase in basicity (atomic weight) of the metal in most of the cases. It is partly due to an increase in the effective weight of the catalyst due to the large amount of deposited metal oxides, these values are also lower than that of pure CeO_2. The decrease in surface area is attributed to the 'dissolution' of the surface by the metals during impregnation, and pore filling by the metal oxides.

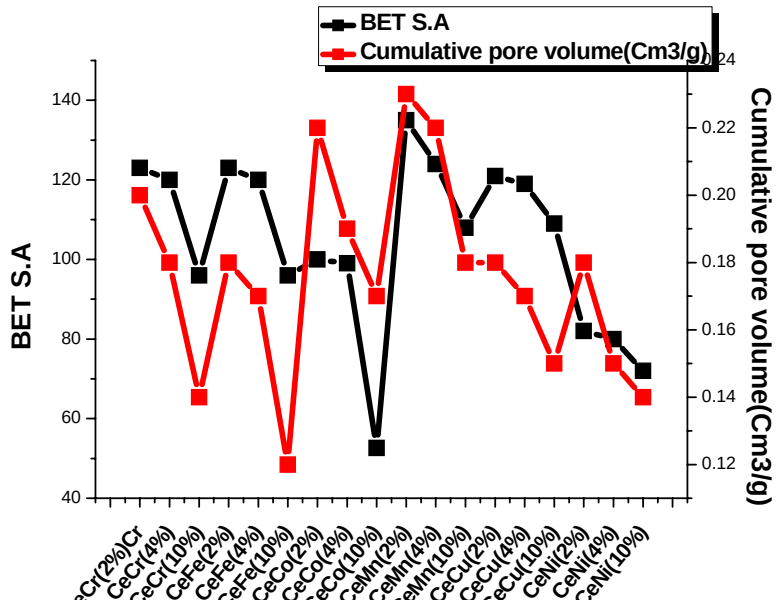

Fig. 3.3 Variation of surface area and pore volume with metal doping

a) Iron incorporated systems

From the Table 3.3 it can be observed that the surface area of the support decreases with the introduction of iron. Surface area decreases on incorporation of 2, 4 & 10 weight% iron into pure ceria. By the incorporation of 10% iron, the surface area is decreased from 100 to 52.6 m^2/g. Pore volume also shows a similar trend when iron is added to pure ceria. The result indicates a negative effect in the surface area on incorporation of iron. It can be inferred that when iron is incorporated into mesoporous ceria by

wet impregnation method, the metal is homogeneously distributed in the system occupying the surface vacant site.

b) Chromium incorporated ceria systems

Table 3.3 shows the effect of chromium doping into mesoporous ceria. The increasing the percentages of chromium, the surface area and pore volume decreases in a similar manner. This also shows the homogeneous distribution of chromium metal into the surface vacant site attained by wet impregnation method.

c) Cobalt incorporated systems

The effect of incorporation of cobalt metal into mesoporous ceria is shown in the Table 3.3. Similar to iron and chromium, cobalt incorporation also decreases the surface area and pore volume with increase in metal %. With increase in the composition of Co from 2 to 10%, the surface area changes from 135 to 108 (m^2g^{-1}).

d) Copper incorporated systems

From Table 3.3 the effect of incorporation of copper into mesoporous ceria can be observed. Though the pore volume and surface area decreases with increase in the percentage of copper, the pore diameter increases initially with metal incorporation, then it decreases when concentration exceeds a certain limit.

c) Manganese incorporated systems

For Mn incorporation the surface area and pore diameter decrease steadily, but the change in the pore volume is not showing the same trend.

e) Nickel incorporated systems

In the case of modification with nickel surface area, pore volume and pore diameter decrease with metal concentration.

3.2.3.1 Nitrogen adsorption isotherm

Fig. 3.4 shows adsorption isotherms of ceria calcined at different temperatures which resemble Type IV of IUPAC classification [3] with a hysteresis loop which is characteristic of mesoporous solids. This hysteresis loop is due to the capillary condensation, in the mesopores. Adsorption at lower relative pressures (p/p_0) is due to the formation of monolayer of nitrogen molecules on the walls of mesoporous material. At low values of P/P_0 the isotherm is similar to Type II, but then adsorption increases rapidly at P/P_0 above 0.5, where pore condensation takes place. This sharp inflection is due to the capillary condensation within the mesopores. From the sharpness of the step corresponding to the filling of the mesopores, once can expect a uniform pore size distribution. The relative pressure corresponding to the inflection point is related to the diameter of the mesopores. In all these cases, the nature of the isotherm at lower relative pressures is same. Though the point of inflection corresponding to the capillary condensation within the mesopores differs, still it is not very significant. In general, for mesoporous materials the presence of hysteresis loop was taken as the confirmation for the presence of mesopores in the material. The N_2 adsorption-desorption isotherms provide information about the mesoscopic nature of the samples.

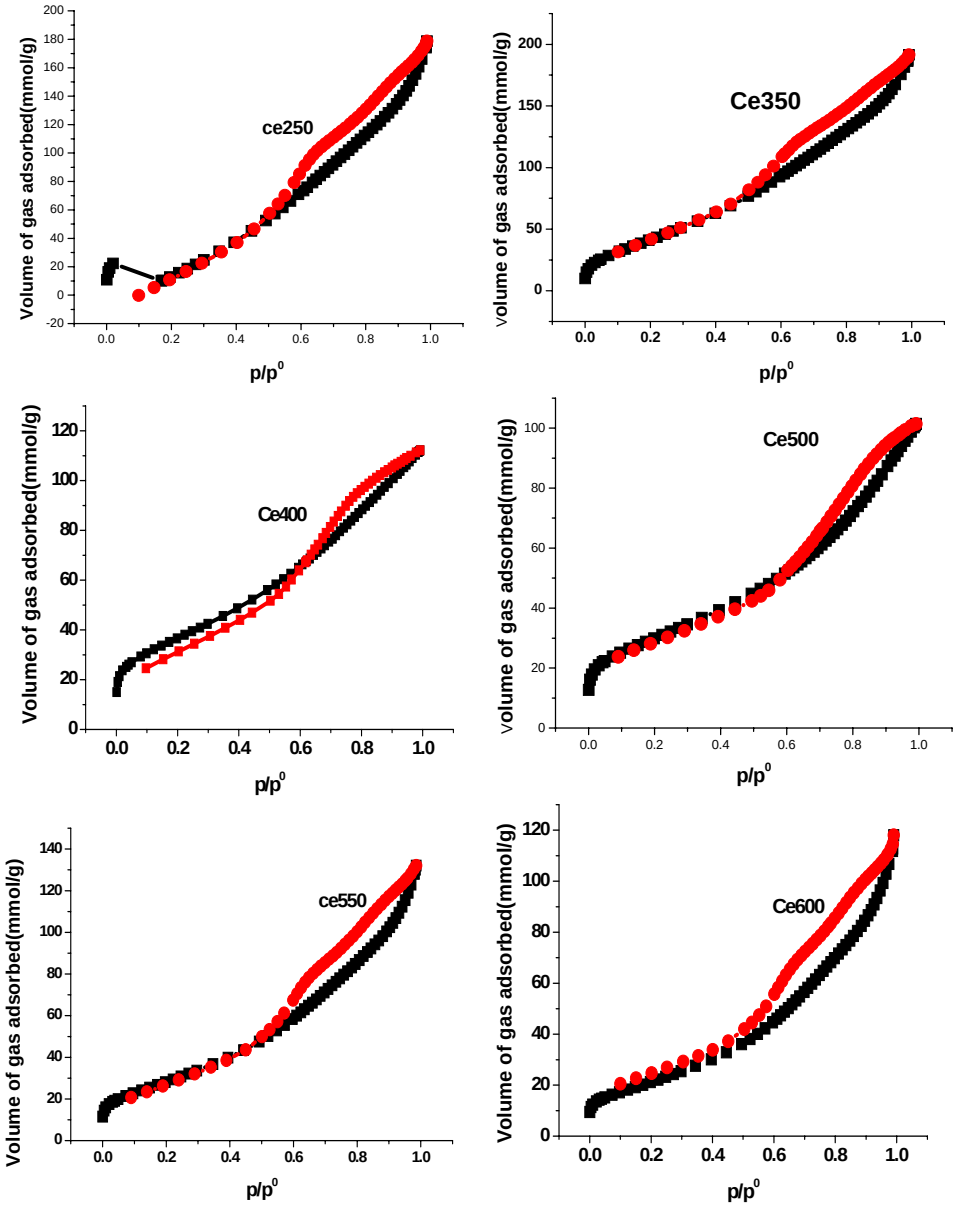

Fig. 3.4. Adsorption isotherms of ceria calcined at different temperatures

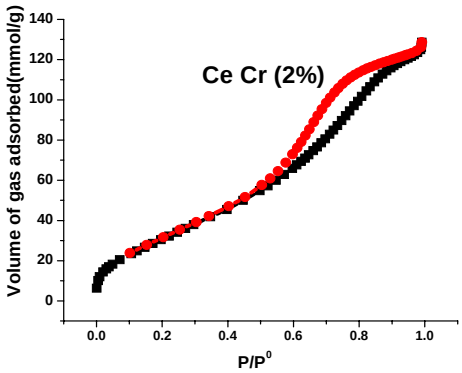
Ce Cr (2%)
Volume of gas adsorbed(mmol/g)
P/P0

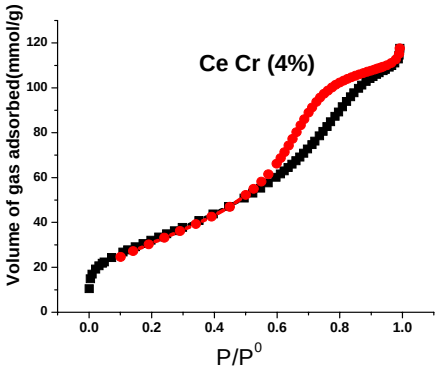
Ce Cr (4%)
Volume of gas adsorbed(mmol/g)
P/P0

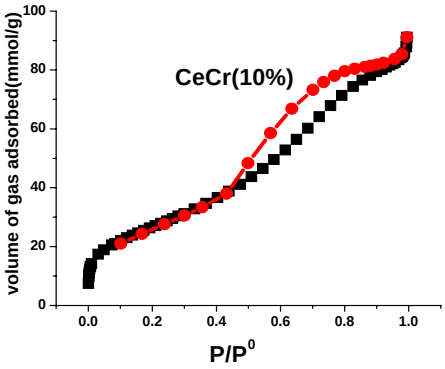
CeCr(10%)
volume of gas adsorbed(mmol/g)
P/P0

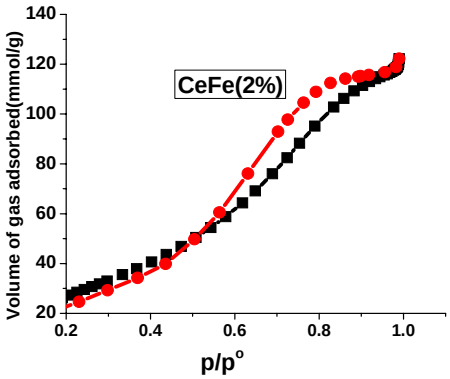
CeFe(2%)
Volume of gas adsorbed(mmol/g)
p/p°

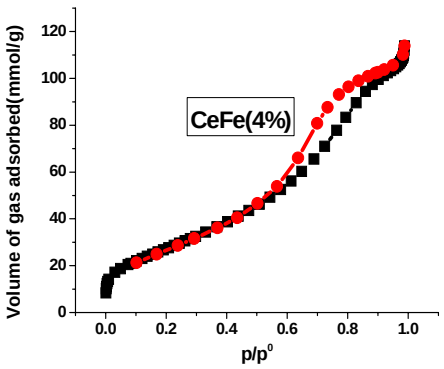
CeFe(4%)
Volume of gas adsorbed(mmol/g)
p/p0

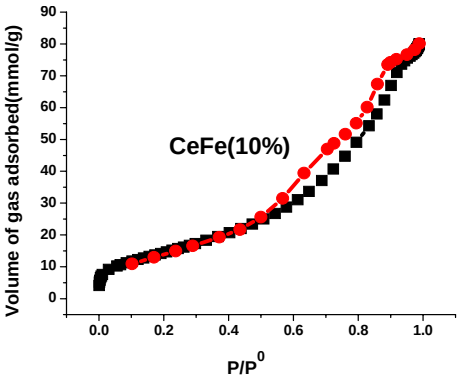
CeFe(10%)
Volume of gas adsorbed(mmol/g)
P/P0

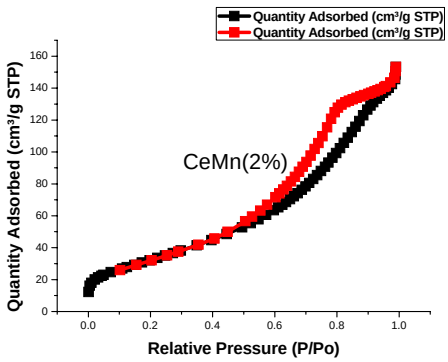
Quantity Adsorbed (cm³/g STP)
Quantity Adsorbed (cm³/g STP)
CeMn(2%)
Quantity Adsorbed (cm³/g STP)
Relative Pressure (P/Po)

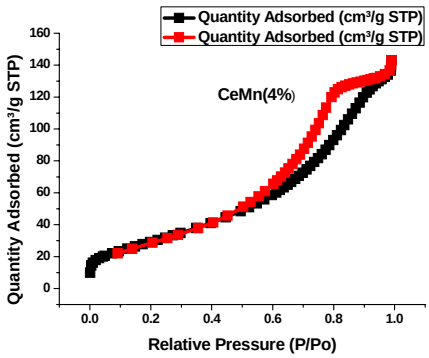
Quantity Adsorbed (cm³/g STP)
Quantity Adsorbed (cm³/g STP)
CeMn(4%)
Quantity Adsorbed (cm³/g STP)
Relative Pressure (P/Po)

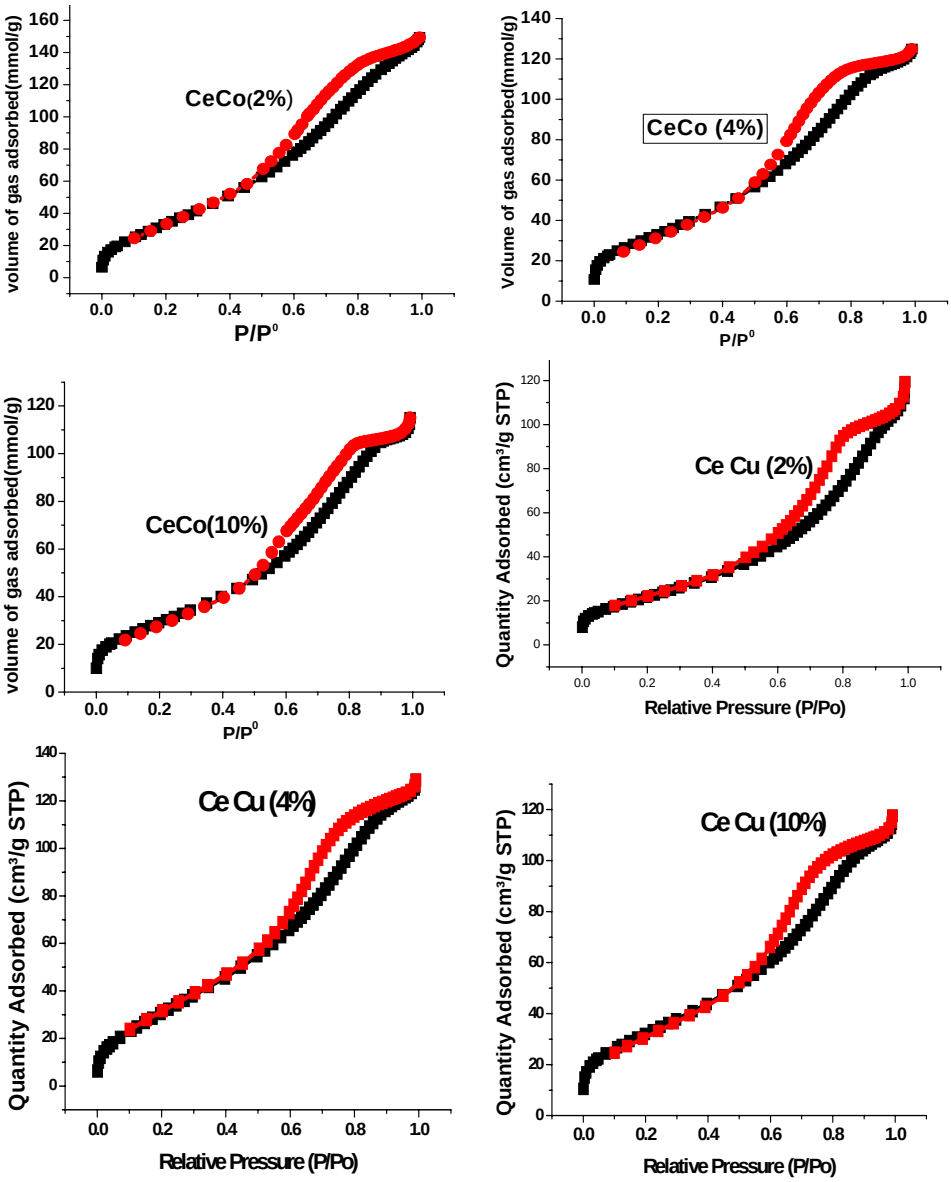

Fig. 3.5. Adsorption isotherms of ceria modified with different metals

3.2.3.2 Pore size distribution

Pore size distribution of calcined mesoporous ceria at different calcination temperatures are shown in Fig.3.6. The values of pore diameter of mesoporous ceria calcined at different temperatures are given in Table3.2. The data show that the pore size is increased when the calcination temperature is

increased from 350 to 500°C, and then it is decreased. This may be due to the rupture of the pore when the temperature is increased. The narrow pore size distribution shows uniformity of the pores.

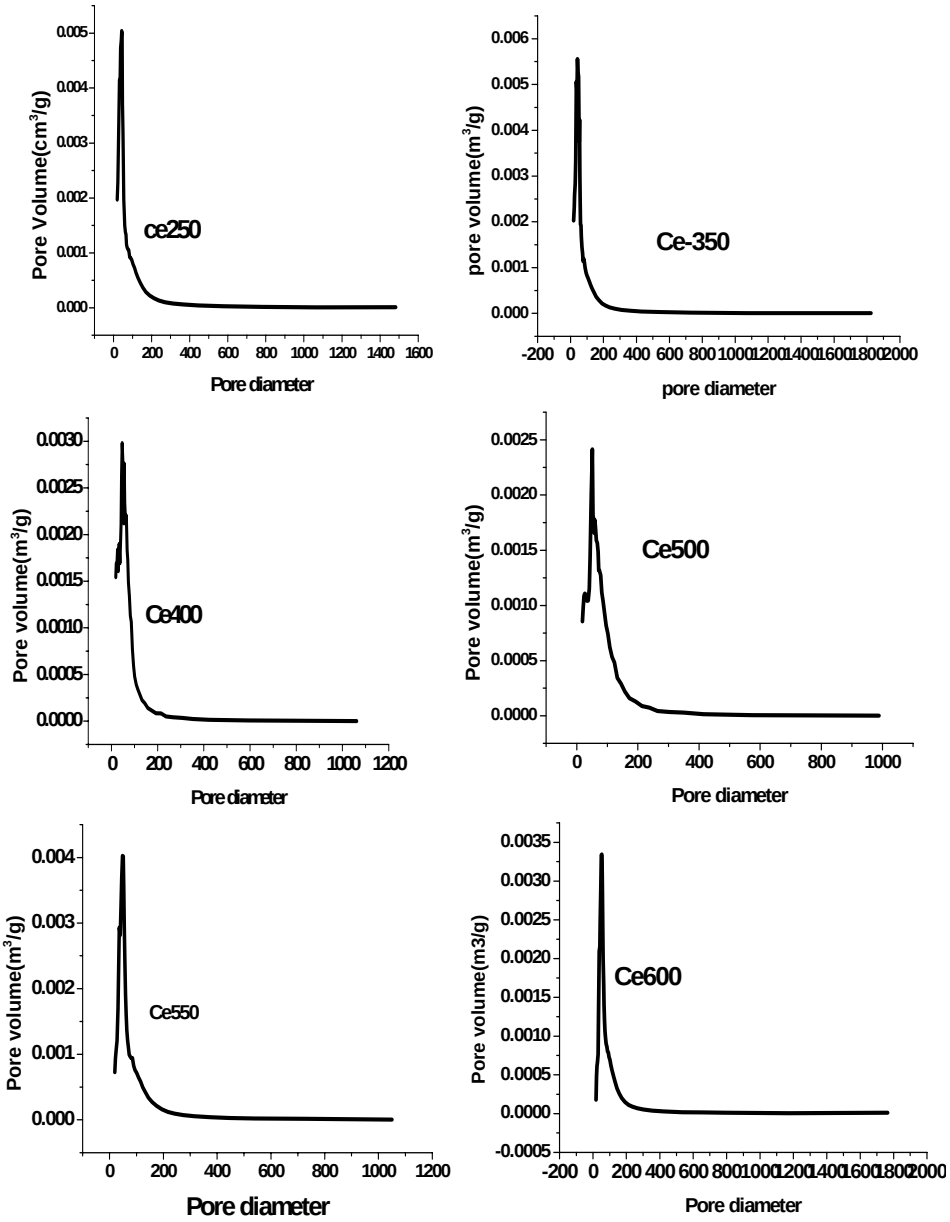

Fig. 3.6. Pore size distribution of mesoporous ceria calcined at different temperatures

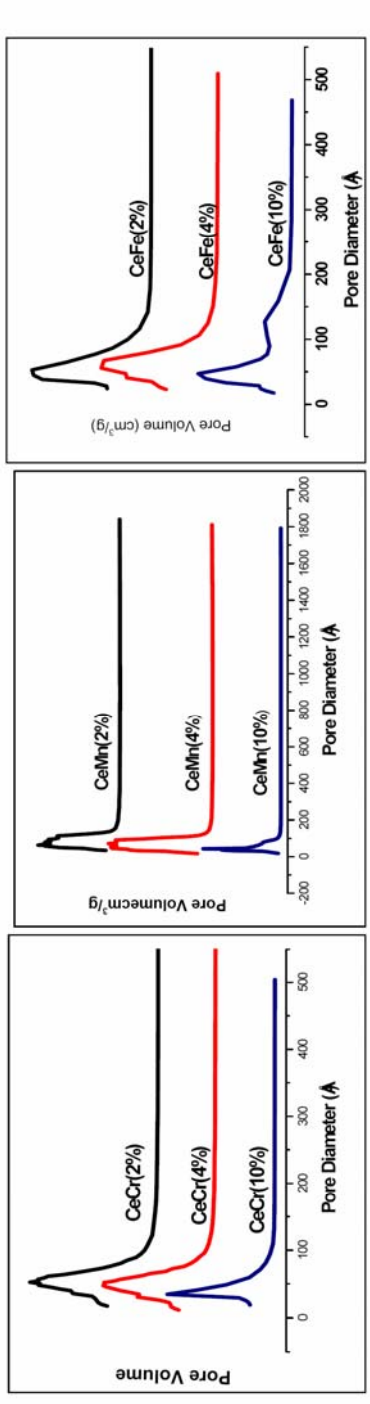

Fig3.7.a

Fig3.7.b

Fig3.7.c

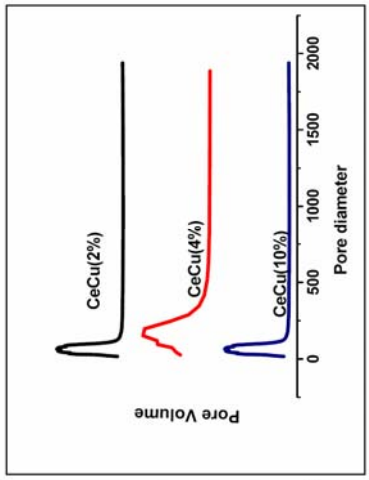

Fig3.7.e

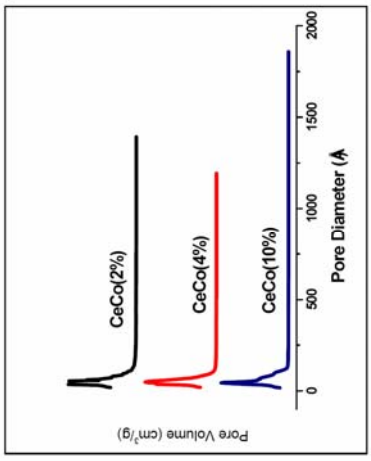

Fig3.7.d

Fig3.7 Pore size distribution of mesoporous ceria modified with transition metals 3.7a. - 2, 4&10% Cr; 3.7b. 2, 4&10% Mn; 3.57c. 2, 4&10% Fe 3.7.d. 2, 4&10%Co; 3.7.e - 2, 4&10%Cu

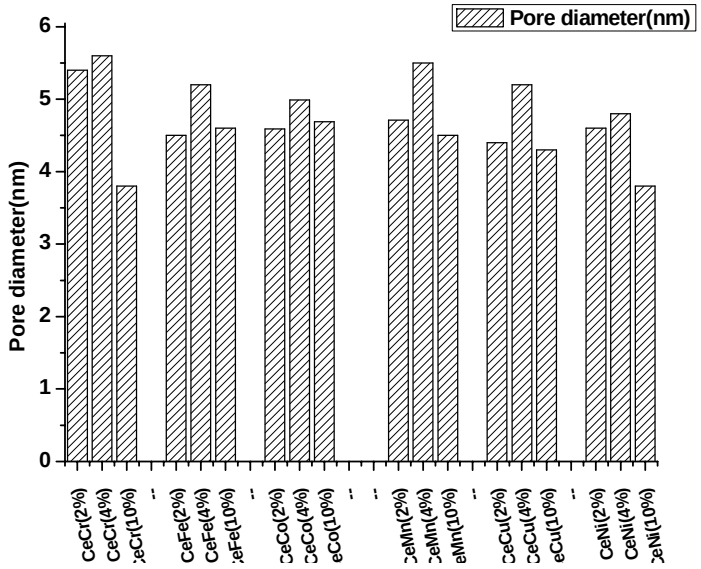

Fig. 3.8 Correlation of metal loading with pore diameter

In Fig.3.8 the pore diameter is correlated with the % metal loading. The pore diameter is increased with metal loading in the sample but only up to a certain percentage. When metal % exceeds a limit the pore diameter decreases.

3.2.4 Wide Angle XRD Analysis.

3.2.4.1 Mesoporous ceria

Fig.3.9.1 illustrates the XRD spectrum indexed from JCPDS database (75-0162). The typical peaks corresponding to the planes (111), (200), (220) and (311) are observed at 2θ = 28.5, 33.0, 47.5, 56.5(^{o}) respectively (space group Fm3m) [4]. Fluorite structure is shown as an inset in the figure. X-ray diffraction within the range of 20-70(^{o}) of calcined ceria at 350^{o}C is also shown. XRD spectra of the prepared ceria consists of all the peaks corresponding to the cubic fluorite structure as is given in the JCPDS file, confirming the cubic crystal structure for ceria prepared by this method.

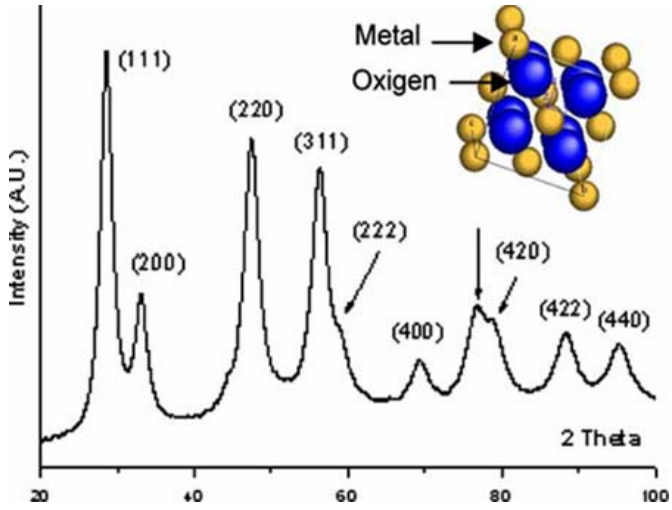

XRD spectrum indexed from JCPDS database 75-0162). Fluorite structure is shown as an inset shown as an inset

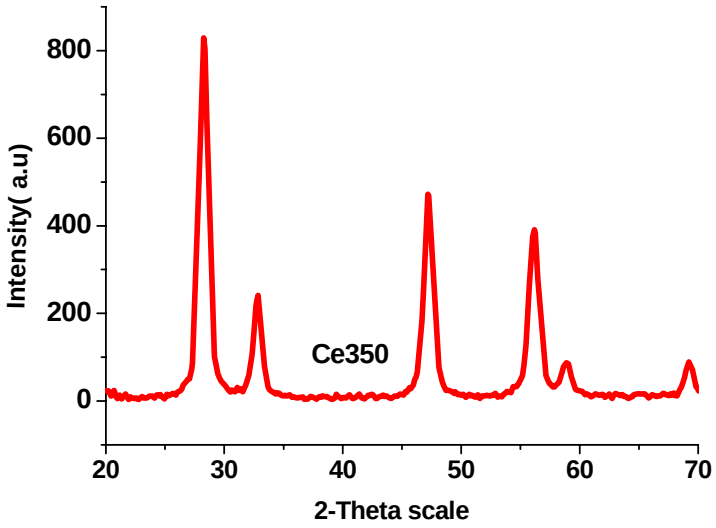

Fig. 3.9.1 XRD spectrum of Ce-350

Fig 3.9.2 represents X-ray diffractograms of ceria calcined at 350^{o}C and pre calcined sample. During the pre-calcination stage itself the phase is formed.

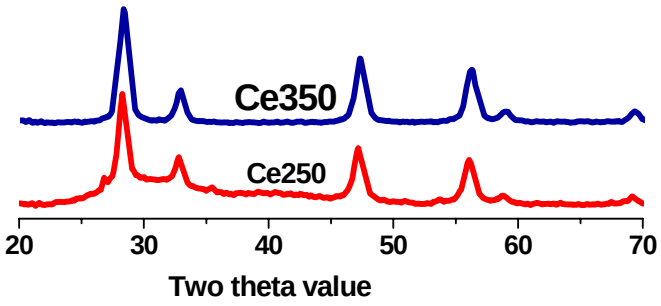

Fig. 3.9.2 X-ray diffractograms of pure CeO_2: Sample pre calcined at 250°C and after calcination at 350°C.

The unit cell parameter is calculated from the d-spacing value using the formula

$$a_0 = d_{111} (h^2 + k^2 + l^2)^{1/2}.$$

Table 3.4 XRD data of ceria calcined at different temperatures

Sample	Average crystallite size (nm)	Lattice parameter(nm)	d-spacing(nm)
Ce250	5.6	5.4	3.127
Ce350	12.8	5.45	3.15
Ce550	10.6	5.46	3.15

Table 3.4 shows the values of crystallize size, and lattice parameters. The increase in the lattice parameter and d-spacing are attributed to the reduction of Ce^{4+} ions (ionic radius 0.97A°) to Ce^{3+} (ionic radius 1.17A°). Average crystallite size is greater for ceria calcined at 350°C.

3.2.4.2 Metal doped samples

The XRD data of the prepared systems agree well with the standard values given in the JCPDS data cards (4 -593) confirming fluorite structure. The mesoporous ceria could effectively induce a good spreading of active phase at its surface, inhibiting the crystallite formation when the metal

loading is lower except for Mn. Though in wide angle XRD pattern characteristic peaks of metal except for Mn are found at higher loading, the intensity of peaks are very low. The absence of peaks of metal oxides indicates that the guest MO_x has been highly dispersed in the support frame work of mesoporous ceria. The typical peaks corresponding to the planes (111), (200), (220) and (311) are observed at 2θ=28.5, 33.0, 47.5, 56.5(^{o}) respectively (space group Fm3m) [4]. After metal incorporation, the presence of all the peaks indicating that the addition of the metal did not destroy the characteristic crystal fluorite structure of ceria. The average crystallite size was calculated using Scherrer equation. For the metal doped samples also the unit cell parameter is calculated from the d-spacing value using the formula

$$a_0 = d_{111} (h^2 + k^2 + l^2)^{1/2}.$$

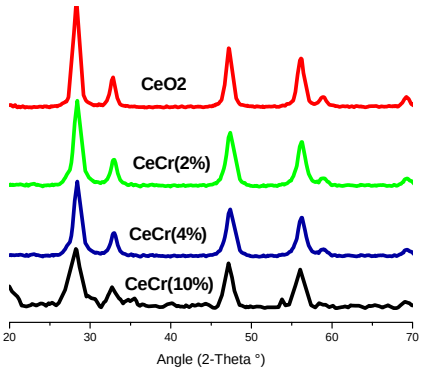

Fig. 3.9.3a

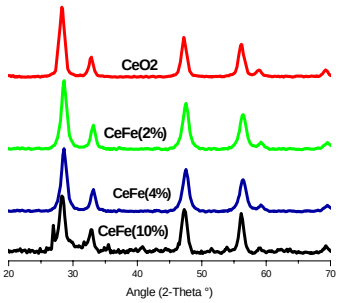

Fig. 3.9.3b

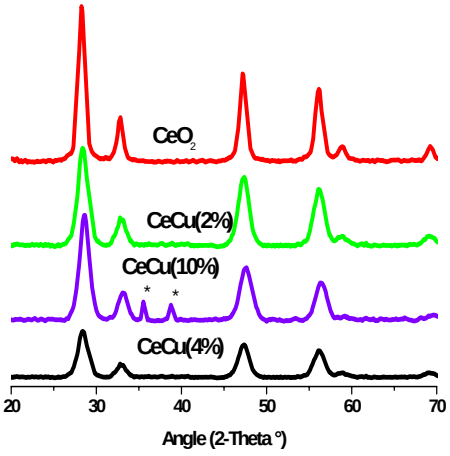

Fig. 3.9.3c

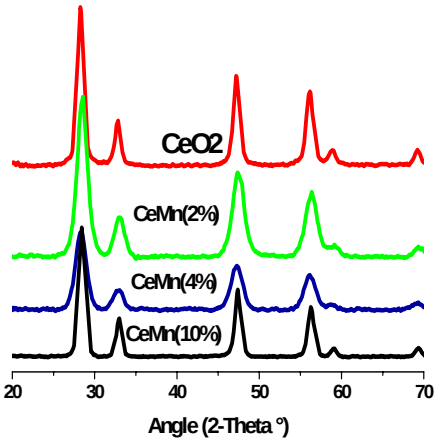

Fig. 3.9.3d

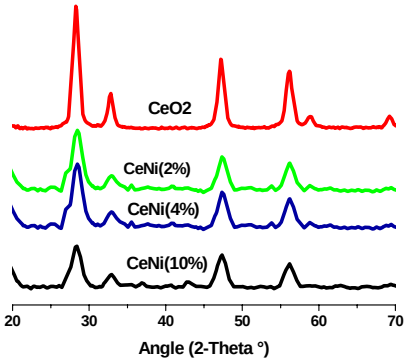

Fig. 3.9.3e

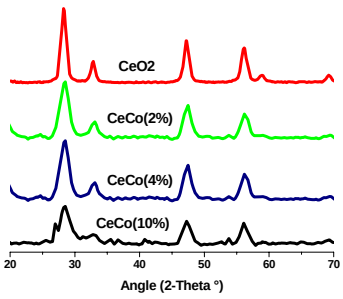

Fig. 3.9.3f

Fig. 3.9.3 XRD patterns of ceria samples of modified with metals

a) **Cr incorporated systems.** The XRD patterns of the modified systems show the peaks corresponding to ceria only (fcc with a = 0.54nm). Cubic fluorite structure of ceria remained intact even after the modification with chromium. The characteristic peak of crystalline chromium oxide is absent in all these cases. It is reported that in the case of metal oxides there is a critical value called dispersion capacity, below which the oxide might become highly dispersed on the support without the formation of its crystalline phase [5]. Since no characteristic peaks corresponding to chromium species is present, it can be concluded that the chromium loading is below the dispersion capacity. According to Viswanath et al., the absence of chromia phase in the diffraction pattern for the supported catalysts may be attributed to the fact that chromium species are randomly dispersed and crystalline size may be smaller than the detection limit [6]. But with higher loading, peaks characteristics of Cr_2O_3 can be found along with the fluorite peaks of CeO_2. Peaks corresponding to 2θ = 24, 33 & 36 are characteristics of Cr_2O_3 species [7]. But in the present case up to 10% loading no chromia crystalline phase is not formed.

b) **Iron incorporated ceria systems.** The powder X-ray diffractograms of the pure and iron doped systems calcined at 350°C is given in Fig. 3.9.3.b. The XRD pattern of pure ceria gives sharp peaks characteristics of the fluorite structure (fcc with a = 0.5435 nm) of ceria, which remained intact after modification with 2, 4 & 10% iron oxide. The characteristic peak of crystalline iron oxide is absent in lower loading. This points to the fact that the iron species are highly dispersed or exist as microcrystalline material below the XRD detection limit as discussed in the case of chromium. But when the

loading is higher than detection limit the peaks corresponding to Fe_2O_3 (2θ = 33, 35 & 54) may be found [8].

c) **Copper incorporated ceria systems.** Table 3.9.3 represents the XRD data indexing results for copper-doped systems. Here the crystallite size increased with modification. The crystal structure is fcc in all catalytic systems. Fig.3.9.3.c represents the X-ray diffractograms of different % of Cu doped mesoporous ceria. In the samples modified with 2 & 4% Copper, no peaks corresponding to crystalline CuO appear. In 10% Cu containing catalyst two peaks corresponding to crystalline CuO were observed (2θ = 35.4, 38.8^o) [9]. So if Cu concentration is higher than 10%, additional CuO crystals will be formed.

d) **Manganese incorporated ceria systems.** Fig. 3.9.3.d. represents XRD spectra of manganese modified systems. It is reported that the replacement of Ce^{4+} crystallites by Mn^{3+} in the fluorite structure is possible by their structural similarity [10]. Manganese oxide crystallisation takes place only when Mn content is greater than 50%. Hence MnO_x are efficiently dispersed on the surface of the catalyst. The addition of manganese ions to ceria or vice versa could help to control crystallite growth and to maintain the pore system of the materials. Similar phenomena were observed in the cases of Mn-Ce catalysts prepared by co-precipitation [11, 12] and combustion method [13] originated from the solid solution formation between Mn_2O_3 and CeO_2, because of their structural similarities. It was well recognized that the dispersion of the active phase plays an important role in the oxidation reaction.

e) **Nickel incorporated ceria systems**. For Nickel modified catalysts, no nickel oxide peaks are seen at Ni loading as shown in Fig. 3.9.3.e. Higher Ni loaded catalyst may show NiO peak at 2θ = 37, 43.7 & 62.9^{o} [14].

f) Cobalt incorporated ceria systems. No formation of crystalline Co oxide was observed in the case of Co (2, 4 &10%) modified systems as shown in Fig. 3.9.3.f. Co loaded catalyst at higher loading may show Co_3O_4 peak at 2θ = 30, 35.5 [8].

Table 3.5 XRD data of ceria modified with transition metals

Sample	Average crystallite size (nm)	Lattice parameter (A^0)	d-spacing (nm)	Scattering Domain size(nm)
Ce350	12.8	5.45	3.15	1.495
CeCr (4%)	9.9	5.43	3.13	0.789
CeCr (10%)	8.66	5.46	3.13	0.789
CeFe (4%)	10.26	5.39	3.12	0.790
CeFe (10%)	10.66	5.44	3.15	0.874
CeMn (2%)	6.27	5.39	3.12	1.054
CeMn (4%)	6.27	5.39	3.14	0.894
CeMn (10%)	12.6	5.43	3.13	0.819
CeCu (2%)	6.93	5.41	3.13	0.843
CeCu (4%)	11.5	5.41	3.13	1.372
CeCu (10%)	6.93	5.38	3.11	1.380
CeNi (2%)	7.1	5.45	3.12	0.691
CeNi (4%)	6.93	5.44	3.14	1.235
CeNi (10%)	6.3	5.44	3.15	0.785
CeCo (2%)	6.9	5.41	3.13	1.293
CeCo (4%)	7.0	5.41	3.13	1.273
CeCo (10%)	6.93	5.41	3.13	1.228

The results obtained on indexing the XRD pattern are given in the Table 3.5. The (h k l) values indicate the fluorite structure of CeO_2. The

crystallite sizes obtained from Scherrer equation shows a decrease with metal incorporation. It is clear that with incorporation of heteroatom in the framework of ceria, a slight decrease in the d_{111} spacing is observed, indicating the presence of the heteroatom within the framework. The cell parameter was calculated using the following equation,

$$a = d_{(111)} \sqrt{h^2+k^2+l^2}$$

One of the interesting features observed in the case of heteroatom incorporated ceria is that with incorporation of heteroatom, the reflections at higher 2θ are not affected. This might be due to the fact that with incorporation of heteroatoms in the framework, the crystallinity of ceria is not changed. This is also observed by various groups who dealt with the incorporation of the various transition metal ions into the framework of mesoporous materials. It is well documented in the literature that with this type of incorporation, the framework order of mesoporous solids decreases because of their semi crystallinity.

3.2.4.3 Low angle X-Ray Diffraction (XRD) Analysis

Small-angle X-ray scattering (SAXS) is a small-angle scattering (SAS) technique where the elastic scattering of X-rays (wavelength 0.1 ... 0.2 nm) by a sample which has inhomogeneity in the nm-range, is recorded at very low angles (typically 0.1-10°). This angular range contains information about the shape and size of macromolecules, characteristic distances of partially ordered materials, pore sizes, and other data. SAXS is capable of delivering structural information of molecules between 5 and 25 nm, of repeat distances in partially ordered systems of up to 150 nm. The mesoporous nature of the ceria samples is confirmed by the low angle XRD pattern (Fig.3.9.4). A Single well resolved peak corresponding to (1 0 0)

plane characteristic of 2D hexagonal structure is obtained. The appearance of low-angle diffraction peaks indicates that mesoscopic order is preserved in the calcined metal oxide materials. For mesoporous materials reflexes are observed in X-ray powder patterns at low 2θ angles ($0.5 < 2\ \theta < 10^{o}$). These reflexes are due to the long-range order induced by the very regular arrangement of the pores. Because d-spacings are rather big for the mesopores, the reflexes appear at low angles.

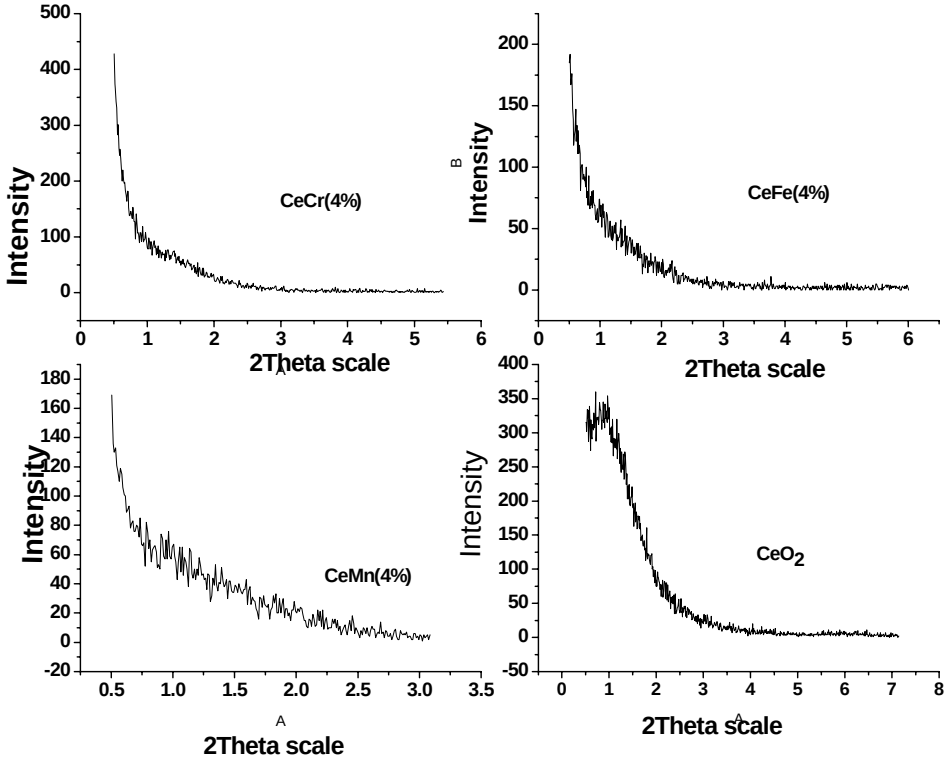

Fig. 3.9.4 Low angle XRD patterns of some representative samples

3.2.5 Scanning electron microscopy (SEM)

SEM analysis of the systems gives us the idea about the surface topography of the catalysts. Fig.3.10 presents the scanning electron micrographs of metal modified systems.

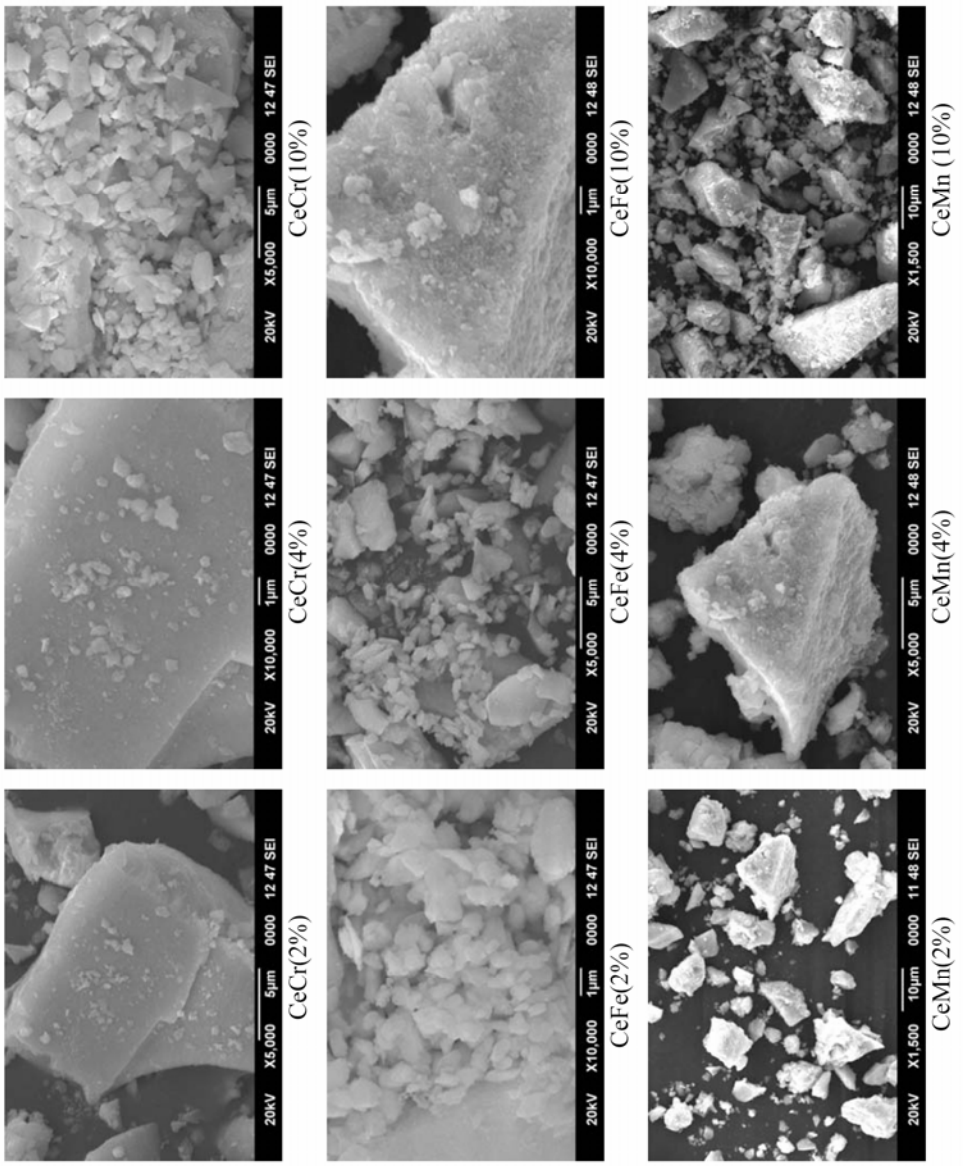
20kV X5,000 5μm 0000 12 47 SEI
CeCr(2%)
20kV X10,000 1μm 0000 12 47 SEI
CeFe(2%)
20kV X1,500 10μm 0000 11 48 SEI
CeMn(2%)
20kV X10,000 1μm 0000 12 47 SEI
CeCr(4%)
20kV X5,000 5μm 0000 12 47 SEI
CeFe(4%)
20kV X5,000 5μm 0000 12 48 SEI
CeMn(4%)
20kV X5,000 5μm 0000 12 47 SEI
CeCr(10%)
20kV X10,000 1μm 0000 12 48 SEI
CeFe(10%)
20kV X1,500 10μm 0000 12 48 SEI
CeMn (10%)

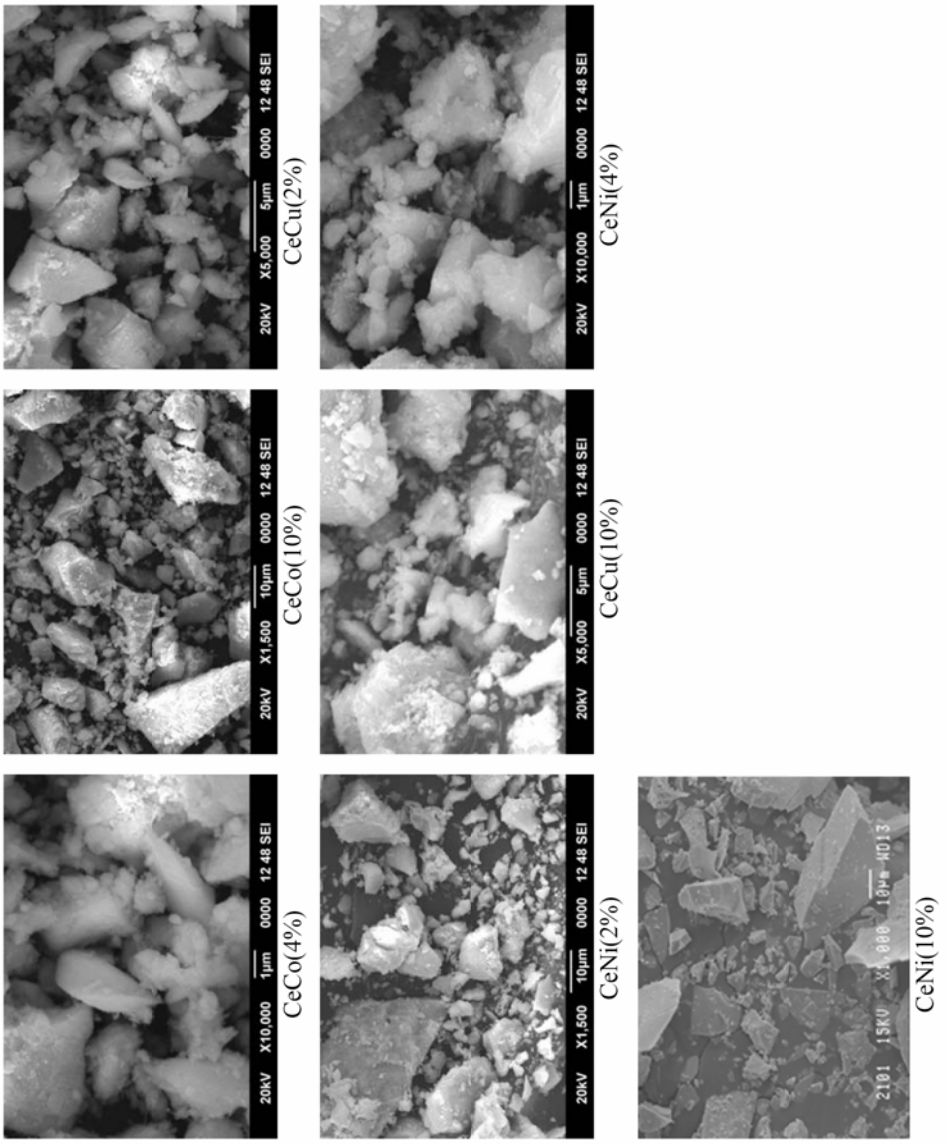

Fig. 3.10. SEM pictures of pure and metal modified mesoporous ceria systems

3.2.6 Thermo gravimetric Analysis (TG/DTA)

To examine the thermal stability of the prepared systems, thermal analysis was carried out and thermogram for pure ceria is shown in Fig 3.11. The mathematically obtained differential curve is also plotted in order to clarify the weight loss processes.

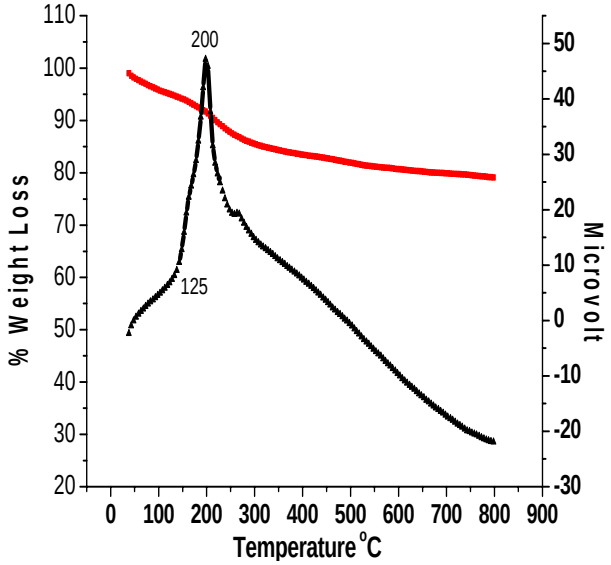

Fig. 3.11 Thermo grams of as prepared ceria

The TG curves of pure ceria show weight loss near 100°C which is due to the loss of physisorbed water as well as water held on surface of the catalyst [15, 16]. The second weight loss around 125-315°C could be due to the elimination of surfactant which is occluded in the mesopores through oxidation process [17]. The TG diagram of the sample shows a decrease of the weight of about 4% up to 100°C and a rapid and continuous weight loss from 125°C to 310°C (nearly 10%). No phase transition is observed indicating the stability of cerium oxide fluorite phase. Very small weight loss due to surfactant indicates the removal of

most of the surfactant during the washing process. Only a small amount of the surfactant is remaining which is to be removed by calcination. This prevents the rupture of crystalline phase and loss of surface area during the high temperature calcination process. No further weight loss is observed confirming the structural stability of the catalyst systems. Mesoporous solids have been associated with severe problems like surfactant removal which in turn reflected on the thermal stability of the final material. In most of the cases, it has been observed that after the removal of the surfactant the pore looks worm-like rather cylindrical (17a). Most important aspect to be considered for the successful synthesis of mesoporous material is the removal of the surfactant. Moreover, compositions other than silica are often more susceptible to hydrolysis, redox reactions or phase transformations, accompanied by thermal breakdown of the structural integrity, which makes it more difficult to remove the template. Here no change is observed indicating the stability of cerium oxide fluorite phase after the surfactant removal.

3.2.7 Ultraviolet-Visible Diffuse Reflectance Spectroscopy (UV-Vis-DRS)

The diffuse reflectance UV-Vis spectroscopy is known to be a very sensitive technique for the identification and characterization of metal ion co-ordination. The UV-Vis DR spectra of metal doped ceria systems are helpful in identifying the structures of metal species dispersed on ceria surfaces. The UV-Vis DR spectra of various metal modified systems are shown in Fig.3.12a & 3.12b.

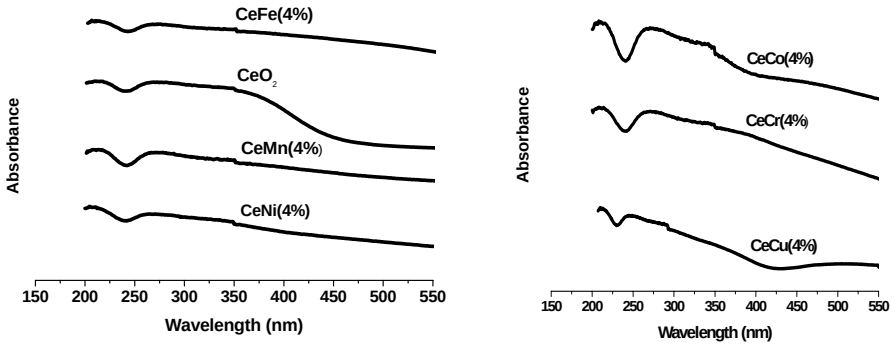

Fig. 3.12a & 3.12b UV-Visible spectra of pure and metal modified mesoporous ceria systems.

The spectrum clearly shows that a single band arising from ceria species around 270 nm is found in all cases. No additional bands are observed by the addition of metals. Since the absorption bands are around 270 nm it is assumed that the Ce^{4+} species are in the tetra co-coordinated environment. The 5d-4f transitions occur prominently in the UV region (~200–270 nm) for isolated Ce^{3+} ions on the surface or in other oxide. Several studies confirm the absence of extra framework bulk oxide species through UV-Vis by the absence of a band around 350 nm, which is due to the forbidden d-d transitions. In all the samples, the bands corresponding to d-d transitions are absent indicating the absence of extra framework bulk metal oxide species. This is confirmed by XRD results.

From Fig 3.12a & b it is evident that a single characteristic band around 250 nm is present in all cases. No additional bands are observed by the incorporation of metals. The position of ligand to metal charge transfer (LMCT, $O^{2-} \rightarrow Ce^{4+}$) spectra depends on the ligand field symmetry surrounding the cerium centre. The electronic transition around 270 nm is due to the tetra coordinated environment of Ce^{4+} species.

3.2.8 Fourier Transform Infrared Spectroscopy (FT-IR)

For the mesoporous material, Fourier Transform Infrared spectroscopy (FT-IR) suggested that no organic species were present after calcination although the surface was covered by adventitiously adsorbed hydroxyl and carbonate species derived from ambient storage of the samples. No FT-IR evidence of superoxide or peroxide formation on the ceria surface, (characteristic vibrational frequencies of 1126 and 883 cm^{-1}, respectively), was found. FT-IR spectra of as prepared ceria and mesoporous ceria calcined at 350^{o}C are shown in Fig. 3.13. The broad absorption band located in the area from 3200 to 3600 cm^{-1} approximately corresponds to the O-H stretching vibration, and the one located in the area from 400 to 750 cm^{-1} to the CeO_2 stretching vibration. The absorption peaks at 1629 and 1062 cm^{-1} correspond to the H_2O bending vibration and Ce-OH stretching vibration respectively [18]. From IR spectra it was found that, the broad band in the range 3000-3500 cm^{-1} is due to the v (O-H) vibrations of H_2O absorbed by the powder sample.

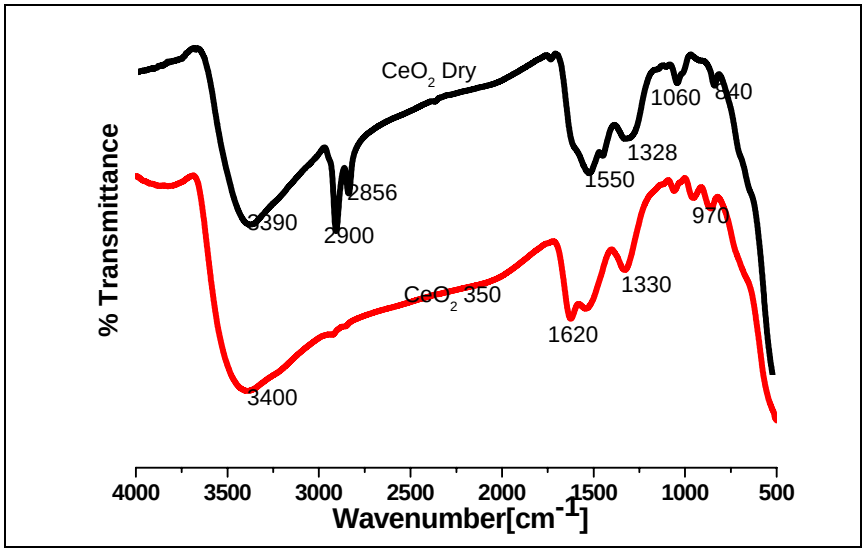

Fig. 3.13 FT-IR spectra of dry and calcined ceria samples.

The band at 1580 cm^{-1} is due to the deformation vibration mode of water (δ-OH). Characteristic peak at 1075 cm^{-1} is attributed to the vibrations of Ce-O-Ce bonding. Moreover no characteristic absorption peak is found at 1384 cm^{-1}. It means that, nitrates are completely removed during filtration and washing. In the spectra, we can find the absorption peaks at 860 cm^{-1}, 665 cm^{-1} and 529 cm^{-1}which are due to stretching and bending mode of vibrations of metal-oxygen-metal bond. For the prepared mesoporous materials, Fourier Transform Infrared spectroscopy (FT-IR) suggested that no organic species are present after calcination, though the surface was covered by adsorbed hydroxyl and carbonate species derived from ambient storage of the samples. No FT-IR evidences of superoxide or peroxide formation on the ceria surface, with characteristic vibrational frequencies of 1126 and 883 cm^{-1}, respectively, were found.

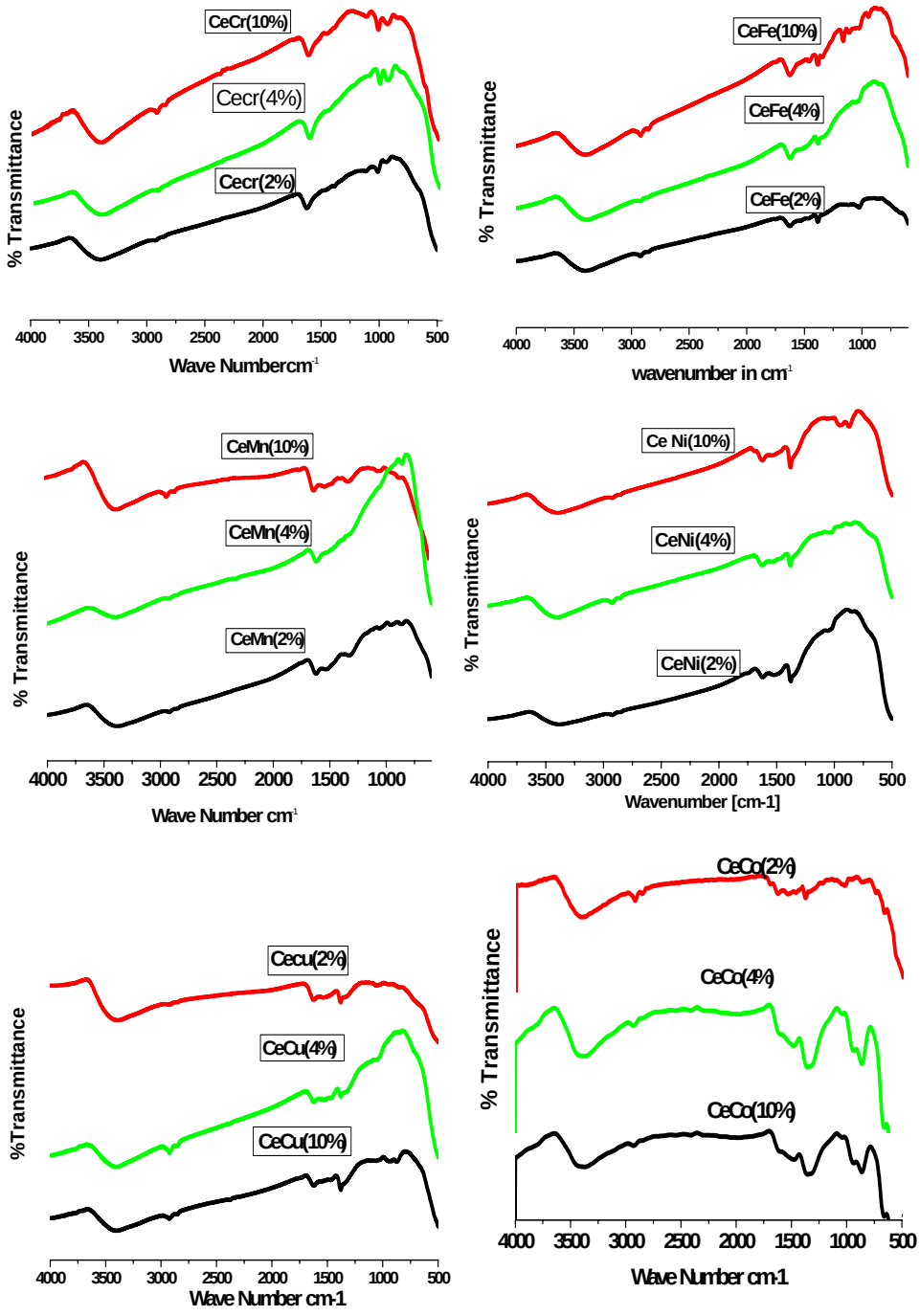

Fig. 3.14. FT-IR spectra of metal doped mesoporous ceria samples.

3.2.9 TEM

To investigate the morphology of the ceria sample the materials were examined by HR-TEM. Calcined sample consists of aggregated small crystallites of a few nanometres and very homogeneous in size. The observed crystallite size is consistent with the calculated value using the Scherrer equation. Also, the selected area electron diffraction (SAED) pattern (Fig. 3.15f) confirms the formation of the (111) surface plane. Ceria crystallizes in a cubic fluorite structure and exposes the thermodynamically most stable (111) surface. This surface is the oxygen termination of stoichiometric O–Ce–O trilayers stacked along the (111) direction and also represents the major fraction of the catalytic surface in the ceria nanocrystallites. Images show the presence of intracrystalline mesoporosities in the material (Fig.3.15a-d). The lattice fringes visible in the HR-TEM image displayed in Fig. 3.15.f are indicative of the high crystallinity of these particles. The indexing of the lattice parameters of the selected area electron diffraction (SAED) shown in Fig. 3.15.f would agree with the structure proposed from the XRD results. The average size of the mesopores between primary nanoparticles is also a few nanometres, which is in accordance with BJH pore size distribution confirms that the particles are single crystallites and not polycrystalline. It can be seen that the particle size of CeO_2 is about 10 nm, which is quite close to the value obtained from the Scherrer equation. The TEM images also reveal aggregates of primary particles.

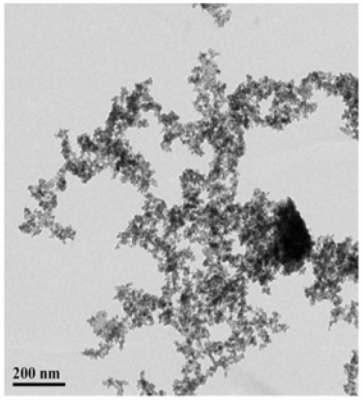

Fig.3.15a. Detailed image of the nanoparticle CeO_2-350 array

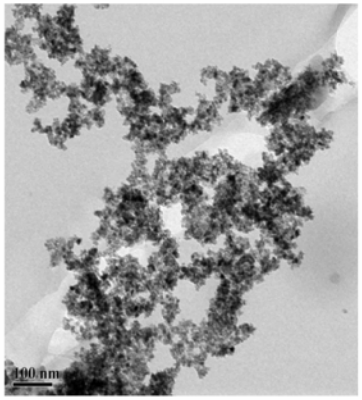

Fig.3.15b. Detailed image of the nanoparticle of CeO_2-350 array

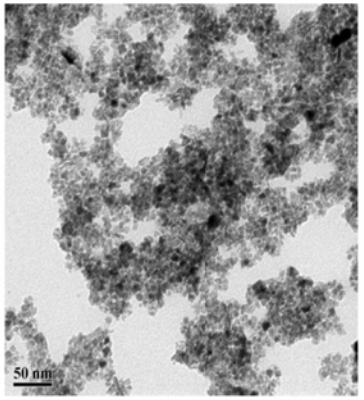

Fig.3.15c. Detailed image of the nanoparticle of CeO_2-350 array

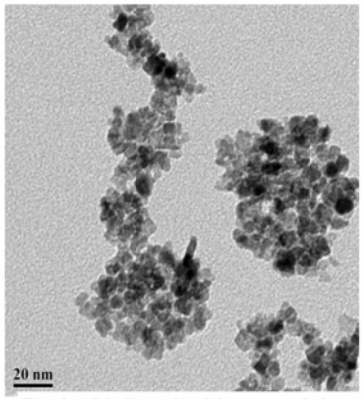

Fig.3.15d. Detailed image of the nanoparticle array

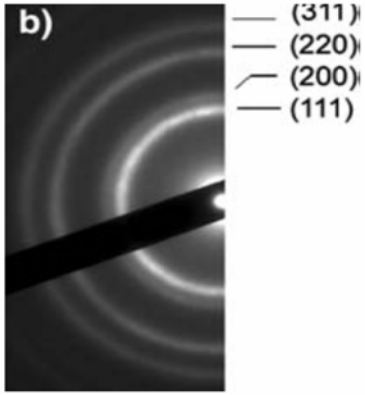

Fig.3.15e. SAED patterns indexed from JCPDS database (75-0162)

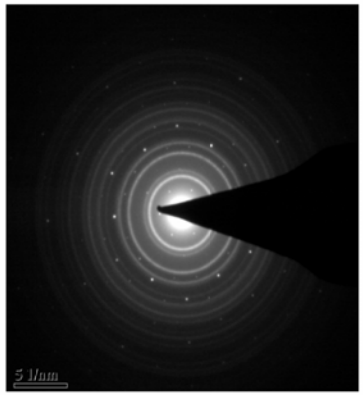

Fig.3.15f. SAED patterns of CeO_2-350

3.2.10 Temperature Programmed Reduction in H_2

(TPR) is unique to study the temperature dependence reduction behavior of ceria based materials. The reduction of ceria takes place essentially in two temperature regions. These two reduction regions are characteristics of ceria and are attributed to the surface and bulk reduction respectively. The coordinately unsaturated surface capping oxygen ions can be easily removed in the low temperature region. However, bulk oxygen requires to be transported to the surface before their reduction. Consequently, the bulk reduction takes place at higher temperature compared to the surface reduction. A linear correlation has been observed between the surface area and the hydrogen consumption at the low temperature region [18a]. The reducibility of the carrier of supported metal catalysts is a very important issue in connection with its ability to generate oxygen vacancies and transfer the oxygen onto the metal particles.

Temperature-programmed reduction (TPR) was carried out in a Micromeritics Instrument: Chemi Soft TPx V1.02 TPR system and 0.1725 mg sample was used for each measurement. Prior to the reduction, the sample was pretreated in an air stream at room temperature for 30 min. After that, H_2-N_2 mixture (5% H_2 by volume) was switched on and the temperature was increased linearly at a rate of $10^oC\ min^{-1}$. A thermal conductivity cell detected the consumption of H_2 in the reactant stream.

Another important aspect to be noticed from figure 3.16 is that the hydrogen consumption in the low temperature region increases with the surface area of the ceria sample. A linear correlation has been observed between the surface area and the hydrogen consumption at the low temperature region. The presence of a variety of surface capping oxygen

ions can be expected in a small crystallite of ceria. A small crystallite surface may contain O^{2-} ions at different positions with different coordination numbers. For example, the oxide surfaces can have imperfections such as steps, kinks, and corners projecting O^{2-} ions of different coordination number. The variety and population of such surface O^{2-} ions may increase with surface area [18a].

The promoting effect of solid solutions in a catalyst for catalytic reaction is based on the improving reducibility of catalyst and the high dispersion of metal oxide on the surface of support, thus accounting for the enhanced catalytic activity of the modified catalyst. There is a correlation between the catalytic properties of catalyst with the reducibility of metal oxide and CeO_2.

It is apparent that the reduction peak shifted towards lower temperature for modified catalysts shows improvement in the reducibility and the area under the peak indicates that large amount of oxygen existing in the catalyst which will be advantageous for the complete oxidation reaction.

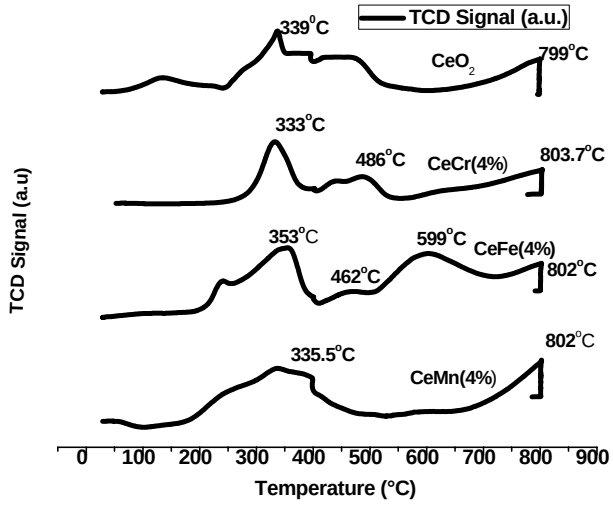

Fig.3.16 TPR profiles of mesoporous CeO_2 and some modified samples

3.3 Surface Acidity Measurement-TPD of ammonia

Metal Oxides due to their ability to take part in the exchange of electrons, protons and oxide ions are used as catalysts in the redox and acid-base catalysis. The acid site is due to the charge imbalance arising between host metal ion and doped metal ions and the basic sites are due to the presence of surface lattice oxide ions. The TPD of ammonia was used to characterize the acid site distribution and furthermore to obtain the quantitative amounts of the acid sites in the specified temperature range [19]. Ammonia is an excellent probe molecule as it allows the distribution of both the protonic and cationic acid centers. In this method, the interaction of acid sites and basic probe molecule (NH_3) is studied to determine the amount and strength of the acid sites [20]. The acid site distribution pattern can be classified into weak (desorption at 100-200^oC), medium (201-400^oC), and strong (401-600^oC) acid sites. The amount of ammonia desorbed at 100^oC may contain some amount of physisorbed ammonia too.

Table 3.6 Distribution of acid sites of pure ceria and transition metals incorporated ceria.

Sample	Weak [mmol/g] (100-200℃)	Medium [m mol/g] (201-400℃)	Strong [mmol/g] (401-600℃)	Medium + strong	Total [mmol/g] (100-600℃)
Ce	0.10	0.02	**Nil**	0.021	0.12
CeFe(2%)	0.09	0.07	0.01	0.08	0.17
CeFe(4%)	0.11	0.02	0.03	0.05	0.16
CeFe(10%)	0.09	0.02	0.02	0.04	0.13
CeCr(2%)	0.11	0.05	0.03	0.09	0.19
CeCr(4%)	0.13	0.02	0.02	0.04	0.17
CeCr(10%)	0.37	0.02	0.01	0.03	0.40
CeMn(2%)	0.07	0.02	0.01	0.03	0.10
CeMn(4%)	0.05	0.01	0.01	0.023	0.07
CeMn(10%)	0.08	0.02	0.01	0.03	0.11
CeCo(2%)	0.1	0.01	0.01	0.02	0.12
CeCo(4%)	0.07	0.015	0.01	0.022	0.09
CeCo(10%)	0.05	0.05	0.02	0.07	0.12
CeNi(2%)	0.13	0.03	0.02	0.05	0.18
CeNi(4%)	0.09	0.01	0.003	0.013	0.10
CeNi(10%)	0.16	0.01	0.01	0.02	0.18
CeCu(2%)	0.15	0.01	0.002	0.01	0.16
CeCu(4%)	0.15	0.02	0.01	0.03	0.18
CeCu(10%)	0.23	0.04	0.03	0.07	0.30

Table 3.6 gives the distribution of acid sites of pure and transition metals incorporated ceria samples. Total acidity is shown as the sum of amount of ammonia desorbed from the entire temperature range.

The table indicates that pure ceria possesses low surface acidity. Upon modification with metals, there is enhancement in the amount of

weak, medium and strong acid sites. But within the series as the metal concentration increases though there is a change in the total acidity, for all the metals there is no steady increase in the acidity with increase in the concentration of the metals.

With iron doping the total acidity is decreased with increase of metal percentage. Tanabe et al. proposed a mechanism for the generation of acid sites by mixing two oxides [21-22]. They suggested that the acidity generation is caused by an excess of positive charge in a model structure of a binary oxide related to the co-ordination number of a positive element and a negative element.

Table 3.6 shows the acid strength distribution of the simple as well as chromium incorporated ceria systems. Here also pure cerium oxide exhibits lowest surface acidity among the different systems. Considerable enhancement of weak, medium, strong acidity is observed after chromium incorporation. Among chromium-modified systems, CeCr (10%) systems have the highest acidity. The TPD data of the chromium oxide doped ceria systems points to an increase of strong acid sites than the simple system. Among the different metals loaded systems (Fe, Cr, Mn, Cu, Co & Ni), Cr doped systems have highest acidity.

For manganese doped systems, the total acidity decreases with increase of concentration of manganese up to 4% then it increases. With Co doping there is not much change in the acidity, but the acidity slowly increases with doping. When Cu is incorporated, the acidity increases in a linear manner with increase in concentration of Cu. With Ni modification, the trend is opposite to that of Mn. Up to 4% the acidity increases; afterwards it decreases with metal doping.

3.3.1 Vapour phase cumene cracking reaction

Vapour phase cumene cracking reaction is a model reaction for identifying the Lewis / Brönsted acid ratio of a catalyst. During cumene cracking over the acidic sites cumene is either dealkylated or dehydrogenated depending on the nature of the acid site present. The major reactions taking place during the cracking of cumene are dealkylation to give benzene and propene over BAS [23, 24] and dehydrogenation to give α-methyl styrene over LAS [25]. A comparison of the amount of dealkylated products and α-methyl styrene gives an idea about the BAS and LAS possessed by the catalyst [26]. It is possible to correlate the acidic properties of the catalysts with the conversion of cumene and with the product distribution of the reaction. The catalytic activity of solid acid catalysts is not only related to the surface concentration of acid sites, but also to their nature, that is being Lewis or Brönsted sites [27]. Vapour phase cumene cracking is a model reaction for identifying the Lewis and Brönsted acid sites present in a catalyst [28]. Fig. 3.17 represents the general scheme of the cumene cracking reaction. So cumene cracking enables a simultaneous determination of Brönsted and Lewis acidity of the catalysts.

In the present work, the vapour phase cumene cracking reaction was carried out in a fixed bed, down flow vertical glass reactor inside a double zone furnace. 0.25g of the catalyst activated at 350^{o}C for 1hr was immobilized inside the reactor with glass wool. The catalyst was loaded in the middle of the reactor and packed with glass beads. The temperature was measured by a thermocouple placed in the middle of the catalyst bed. Cumene was fed into the reactor at a flow rate of 4mL/h after optimization. The temperature of the reaction bed was kept at 500^{o}C.

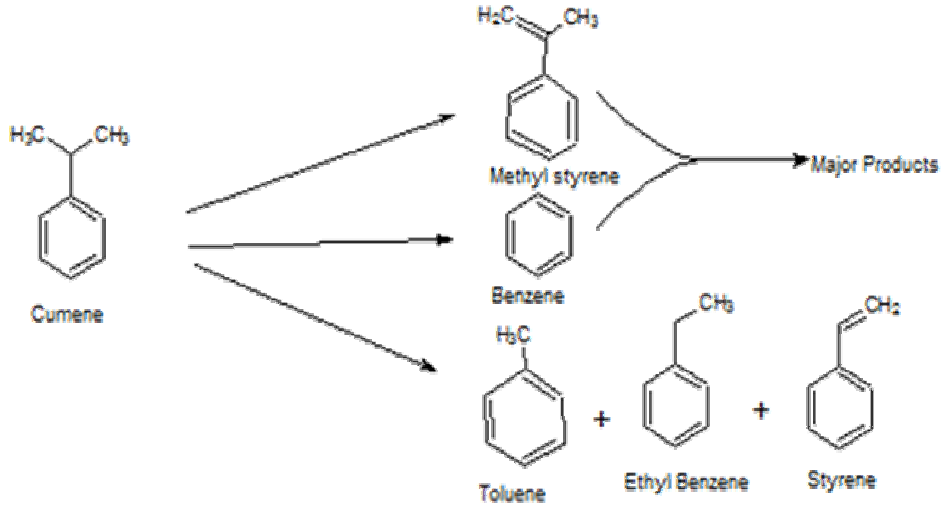

Fig 3.17 Reaction scheme of vapour phase cumene cracking

The product analysis was achieved by gas chromatography (Chemito GC 1000) by comparison with authentic samples. The analytical conditions are given in the table.

3.3.2 Optimization of reaction conditions

The influence of reaction conditions such as temperature, flow rate and time on stream on the conversion and selectivity is investigated. The results are given in the following sections.

3.3.2.1 Effect of Temperature

For the optimization of reaction temperature, the catalytic activity was measured at different temperatures such as 350, 400, 450 and 500^{o}C with a constant flow rate of 4 mL/h for 2 hours.

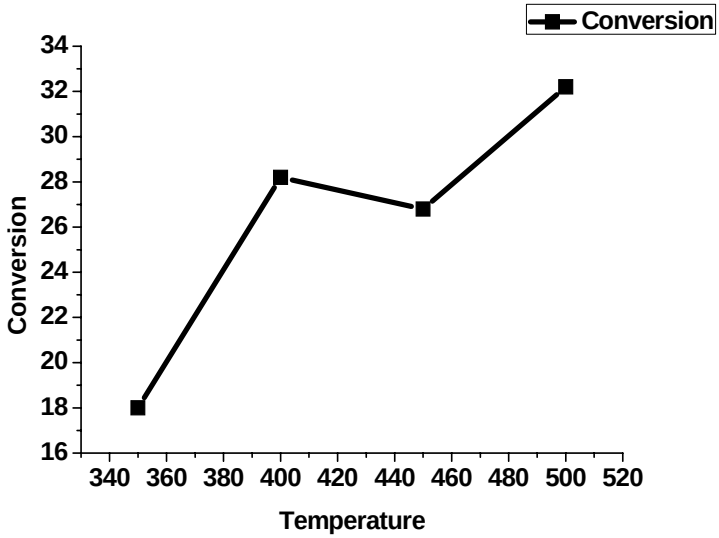

Fig. 3.18 Effect of Temperature on cumene cracking

Reaction condition: Catalyst: 0.25g CeCr (10%), Flow rate 4mL/h, Time: 2h

The result shows that as the temperature increases the cumene conversion also increases. At higher temperature the possibility of cracking of the carbon chain increases.

3.3.2.2 Effect of flow rate

The optimization of flow rate was done by performing the reaction at different flow rates like 4, 5, 6 and 7 mL/h at a constant temperature of 500^{o}C for 1 hour. With regard to flow rate, higher flow rates were found to reduce the percentage conversion. This is because of the lower residence time of the reactants on the catalyst surface. It is reported that a decrease in the conversion is observed at higher flow rates due to smaller contact time, where the kinetics get affected [29].

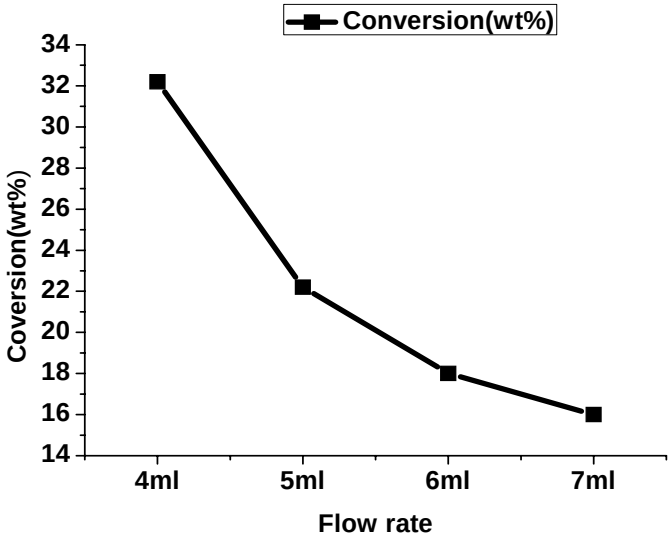

Fig. 3.19 Effect of flow rate on cumene cracking

Reaction condition: Catalyst: 0.25gCeCr (10%), Flow rate 4mL/h, Time: 2h, Temperature: 500^{o}C

3.3.2.3 Effect of time of flow

Table 3.7 Effect of time of flow

Catalyst: CeCr (10%) Temperature:500^{o}C Weight: 0.25g Flow rate:4mL	**Flow rate**	**Conversion (wt %)**
	1hr	31
	2hr	32.2
	3hrs	33
	4hrs	28

To study the effect of time on stream, the reaction was carried out continuously for 4 hours over catalyst CeCr (10%) at a temperature of 500^{o}C and a flow rate of 4 mL/h. The effect of contact time on the conversion and selectivity towards dehydrogenation and cracking products is shown in Fig. 3.18. Although an increase in the percentage conversion of cumene can be seen in the beginning of the reaction, the

conversion is found to decrease as time proceeds. It is a known fact that during organic reactions catalyzed by solid acid catalysts, the catalyst always suffers from strong deactivation due to formation and retention of heavy by products, so-called coke, which deactivates acid sites [30]. Wang and Manos [31] observed a similar decrease in product conversion with time during the reaction of 1-pentene over different zeolite catalysts. According to them, the drastic decrease in conversion seen during the reaction indicates a rapid coke formation, which takes place on acid sites catalyzing the reaction. Similarly, in the present reaction, the decrease in percentage conversion with reaction time may also be due to the blocking of the acid sites by the coke formed during the reaction. It is reported that the acid sites are strong promoters for coke deposition and deactivation of the catalyst [32].

Table 3.8 Optimized Conditions

Temperature	500^{o}C
Weight	0.25g
Flow rate	4mL
Temperature	500^{o}C

3.3.2.4 Effect of various catalysts on cumene cracking

Comparison of the catalytic activity of different systems was done at a temperature of 500^{o}C with a flow a rate of 4 mL/h for 1 hour. The products were identified using a gas chromatograph (GC 1000 Chemito with an SE- 30 capillary column). The injector and detector temperature of GC was maintained at 230^{o}C and the temperature programme for the column is set as 70^{o}C-2min-10^{o}C/min-250^{o}C-2min.

Table 3.9 Comparison of catalytic activity of different samples on cumene cracking reaction

Sample	Cumene Conversion	α-methyl styrene selectivity	Dealkylated products selectivity	Lewis/ Bronsted acidity
CeFe (2%)	18.5	74	26	2.8
CeFe (4%)	27	62.6	37.4	1.7
CeFe (10%)	14.2	57.2	42.8	1.3
CeCr (2%)	31.6	59.7	40.3	1.5
CeCr (4%)	22.5	58	42	1.4
CeCr (10%)	31.8	67.2	32.8	2.0
CeMn (2%)	24.8	65	35	1.9
CeMn (4%)	14.6	64.5	35.5	1.8
CeMn (10%)	25	68.2	31.8	2.1
CeCo(2%)	26	68	32	2.1
CeCo (4%)	28	67	33	2.0
CeCo (10%)	30	66.6	33.4	1.99
CeNi (2%)	33	68.2	31.7	2.1
CeNi (4%)	30	45.2	54.8	0.8
CeNi (10%)	20	49.5	50.5	1.0
CeCu (2%)	14	46	54	0.9
CeCu (4%)	24	75.9	24	3.1
CeCu (10%)	31	77	23	3.3

The results show the presence of both Lewis and Brönsted acid sites on the catalyst. α-methyl styrene is the major product along with some dealkylated products. Higher selectivity towards α-methyl styrene for the incorporated systems suggests the enhancement in Lewis acidity upon modification. Since the total acidity of the catalysts increases with incorporation, we can conclude that transition metal ion modification result

in an increase in the Lewis acidity of pure ceria. The higher selectivity towards α-methyl styrene obtained during the reaction suggests the presence of more number of Lewis acid sites compared to the Brönsted acid sites.

3.3.3 Correlation of acidities from TPD of ammonia and cumene cracking reaction

The total acidity of the catalysts as determined by the temperature programmed desorption (TPD) of ammonia is found to influence the percentage conversion of cumene in the reaction. With transition metal ion impregnation, the total acidity of the catalysts was found to increase (as evident from TPD of ammonia) thereby increasing the total conversion of cumene in the reaction. Aberuagba et al. [33] also reported a similar dependence in cumene conversion with total acidity in the case of zirconia-alumina mixed oxides and magnesia-alumina mixed oxides. Since the total acidity of the catalysts increases with incorporation, we can conclude that transition metal ion modification result in an increase in the Lewis acidity of pure ceria.

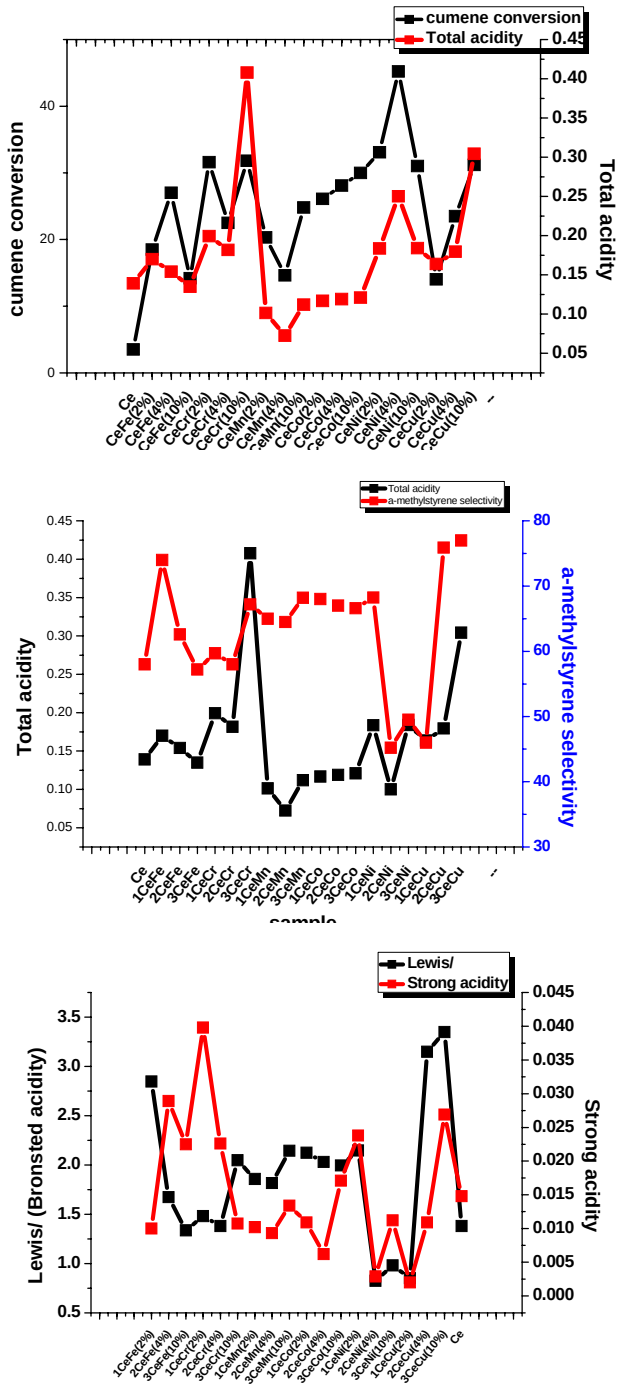

Fig. 3.19. Correlation of acidities from TPD of ammonia and cumene cracking reaction

In the study cumene conversion was found to depend on the surface acidity as obtained from TPD of ammonia. Modified systems are found to be more active than the simple system. Good correlation is observed for total acidity with cumene conversion, total acidity with α-methyl styrene selectivity, and Lewis to Brönsted acidity ratio with strong acidity obtained from TPD of ammonia. Strong acidity from TPD of ammonia may be taken as a measure of Lewis acid site. Lock and co-workers reported that desorption of ammonia in the moderate temperature range is due to potential Brönsted acid sites (BAS) [34]. This supports the generation of BAS through the hydrolysis of cations during temperature treatment.

3.4 Conclusions

The different surface characterization techniques and surface acidity studies may be concluded as:

- Mesoporous ceria modified with various transition metals can be successfully synthesised by template method using hexadecyl amine as surfactant. All the samples prepared have ordered pores.

- As the calcination temperature increases the surface area decreases. Also the surface area and pore volume of the support decrease with the introduction of transition metals. Adsorption isotherms of ceria calcined at different temperatures resemble Type IV of IUPAC classification which is characteristic of mesoporous materials. There is good correlation between surface area and pore diameter of the different sample. The narrow pore size distribution shows uniformity of the pore

- The XRD data of the prepared systems agree well with the standard values for the cubic fluorite structure of ceria. Except for 10% Cu no new characteristic phases where observed with the incorporation of transition metal oxides. This shows that metals are highly dispersed within the frame work structure.
- From FTIR and TG/DTA studies it can be concluded that the neutral surfactant can be successfully removed at a lower calcination temperature attaining maximum surface area.
- The acidity studies interpreted the total acidities of samples with the cumene cracking conversion. Good correlation was obtained between the acidities obtained by vapour phase cumene cracking and Temperature programmed desorption of ammonia. Acidity studies confirm the enhancement of surface acidity in particular strong acidity, upon modification with transition metals.

3.5 References

[1] H. P. Olieveira, F. J. Aaissi and H. E. Toma, *Mat. Res. Bull*., 33(12) (**1998**) 1792

[2] T. Masui, K. Fujiwara, K. Machida, G. Adachi, T. Sakata and H. Mori (**1997**) *Chem. Mater*. 9 2197–204

[3] S. Karera, S. Nargis, Patel M. Patel, *J. Sci. Ind. Res.,* 45 (**1986**) 441.

[4] S. Sato, K. Koizumi, F. Nozaki, *J.catal.*178(**1998**)264

[5] Z. Crnjak Oral, "*Nanoparticles in solids and solutions"* 519(**1996**) Kluwer, Netherlands.

[6] R. P. Viswanath, P. Wilson, *Appl. Catal. A: Gen*, 201(**2000**)23.

[7] Wenbo Yue and Wuzong Zhou, Supplementary Material (ESI) for Journal of Materials Chemistry, The Royal Society of Chemistry 2007

[8] Dan-qing Yu, Yue Liu*, Zhong- biao Wu, J Zhejiang *Univ- Sci A (Appl.Phys & Eng)* in press

[9] Y. Hu, L. Dong, J. Wang, Y. Chen, *J.Mol.Catal.A:Chem162*(**2000**)307

[10] G. Qi, R.T. Yang, *J.Phys.Chem.B*108(**2004**)15738

[11] M. Machida, M. Uto, D. Kurogi, T. Kijima, *Chemical Material*, 12(10) (**2000**)3158-3164

[12] G. S. Qi, R. T. Yang, R. Chang, *Applied Catalysis B: Environmental*, 51(2): 93-106(**2004**)01.023.

[13] B. Murugan, A. V. Ramaswamy, D. Srinivas, C. S. Gopinath, V. Ramaswamy, *Chemical Material,* 17(15): (**2005**) 3983-3993.

[14] Y. Li., Q. Fu, M. Flytzani-Stephalopolous, *Appl.Catal*.B.27(**2000**)179

[15] F. Arena, R. Daris, A. Paramaliana, *Appl. Catal. A: Gen.,* 170 (**1998**) 127.

[16] B. Scheffer, J. J. Heijinga, J. A. Moulijn, *J. Phy. Chem*., 91(**1987**) 4752.

[17] D. Terrible, A. Trovarelli, J. Liorcaet.al. *J.Catal.,*178(**1998**)299

[17a] F. Schuth, *Chem. Mater*. 13 (2001) 3184

[18] K. Tanabe, *Bull. Chem. Soc. Jpn*. 47 (**1974**) 1064.

[18a] Ranga Rao & B. G. Mishra, *Bulletin of the Catalysis Society of India* 2 (**2003**)122-134

[19] L. I. Matienko, L. A. Molosova, Russ. Chem. Bull. 48 (**1999**). 55.

[20] R. Alcantara, L. Canoira, P. G. Joao, J. M. Santos, I. Vasques, *Appl. Catal. A:Gen*., 203 (**2000**) 259

[21] T. Maeda, A. K. Pee, D. Haa, *Chem. Abs.*, (**1995**) 4520.

[22] R. YU, F. Xiao, D. Wang, T. Sun and S. Feng, *Catal. Today,* 51 (**1999**) 39.

[23] T. J. Dines, C. H. Rochester, A.W. Ward, (**1991***) J. Chem. Soc. Farad. Trans*. 87:1611

[24] M. Hino, M. Kurashige, H. Matsuhashi, K. Arata K., *Appl. Catal. A*(*2006*) 310:190–193

[25] A. Gil, L. M. Gandia., M. A. Vicente , *Catal Rev SciEng* **(2000**) 42:145

[26] T. Mishra, K. Parida, *Appl. Catal. A Gen* (**1988**) 174:91

[27] E. Selli, L. Forni, *Micropor. Mesopor. Mater*.(**1999**) 31:129–140

[28] Fincy Patrick, S. Sugunan, *Reac. Kinet .Mech. Cat.* (**2011**) 103:125–131

[29] R. M. Koro, E. J. Novak , *Chem. Eng. Sci.*(**1967**) 22:470

[30] M. Guisnet, P. Magnoux, *Appl. Catal. A*(**2001**) 212:83

[31] B. Wang, G. Manos, *Ind.Eng.Chem. Res.*(**2008**) 47:2948–2955

[32] F. Trejo , M. S. Rana, J. Ancheyta , *Ind.Eng.Chem Res*(**2011**) 50:2715–2725

[33] F. Aberuagb, M. Kumar, J. K. Gupta, G. Muralidhar, L. D. Sharma *React Kinet. Catal. Lett* 80 (2003) 311–317